



Universidade do Minho
Escola de Engenharia

Andreia Bastos Pires de Lima

Study of the tightness of the metallization
used on top of a thin film capacitor cell



Universidade do Minho
Escola de Engenharia

Andreia Bastos Pires de Lima

Study of the tightness of the metallization
used on top of a thin film capacitor cell

Dissertação de Mestrado
Ciclo de Estudos Integrados Conducentes ao
Grau de Mestre em Engenharia de Materiais

Trabalho efetuado sob a orientação do
Professor Doutor Carlos J. M. Tavares
Engenheiro José A. A. Lagido

julho de 2015

DECLARAÇÃO

Nome: Andreia Bastos Pires de Lima

Endereço eletrónico: andreia.bastos.lima@gmail.com Telefone: 961420685

Cartão do Cidadão: 14154948

Título da dissertação: Study of the tightness of the metallization used on top of a thin film capacitor cell

Orientadores:

Professor Doutor Carlos J. M. Tavares

Engenheiro José A. A. Lagido

Ano de conclusão: 2015

Mestrado Integrado em Engenharia de Materiais

DE ACORDO COM A LEGISLAÇÃO EM VIGOR, NÃO É PERMITIDA A REPRODUÇÃO DE QUALQUER PARTE DESTA TESE/TRABALHO.

Universidade do Minho, 31 de Julho de 2015

Assinatura:

To my parents, sister and boyfriend.

ACKNOWLEDGMENTS

During the realization of this master thesis, there were some people that one way or another, contributed for the realization of this work and I want to express my acknowledgements to them.

To professor **Carlos Tavares** for all the orientation, for the scientific suggestions that he provides during the realization of this work and for the support, patience and availability that he showed, even when it was not exactly his area.

To engineer **José Lagido, Vitor Reis** and **Vitor Araújo** that allowed the elaboration of this master thesis in Vishay Electrónica Portugal and for all the technical support, orientation and availability demonstrated during this work.

To **Silvia Santos** for all the support, patience, orientation, advices and availability during this work, even when it was not exactly her function.

To professor **Sandra Carvalho** for providing the equipment for electrochemical corrosion tests and to **Edgar Carneiro, Cristiana Alves** and **Sebastian** for all the support in the analysis of the electrochemical corrosion tests.

To professor **Ana Pinto** to all the advices demonstrated during this work.

To all the Vishay workers and technicians in the physics department of University of Minho that, one way or another, contributed for this master thesis, especially to **Marta, Sr. Marinho** and **Adão Ferreira**.

Particularly, to my **parents (Manuel Lima and Maria Fernanda Lima)** for all the support, patience and for all the work that allowed me to conclude this step.

To my **sister (Maria José Lima)** and **brother in law (Bruno Maia)** for all the support and advices that were useful during this step.

To my **boyfriend (António Leite)** for all the support, patience and encouragement that helped me to conclude this step.

To my **grandparents** and the rest of my **family** for the support and patience that they demonstrated during this step.

To my **friends** for all the support, fellowship, patience and advices that allowed me to conclude this step with a better mood.

ABSTRACT

Vishay Intertechnology Inc. is a worldwide company in electronic components sector. It is a manufacturer of discrete semiconductors and passive electronic components. Vishay Electrónica Portugal Lda in Vila Nova de Famalicão produces film capacitors, which are the main focus of this work. Film capacitors are applied on several electronic equipments and the reliability of the capacitors has a major impact on the operational reliability and maintenance costs of the whole system. To test the capacitors reliability it is used biased 85°C/85% RH test. In this test, the components are exposed at 85°C and 85% relative humidity during 1000 hours. Vishay wants to ensure their customers that the capacitors pass the biased 85°C/85% RH test. In this way, it is necessary to improve the capacitor construction and inherent performance.

A film capacitor is mainly constituted by five parts: film metallization, metallization on top of the cell, terminals, insulating resin and plastic case. During this work, the film metallization and the metallization applied on top of the cell were tested in order to evaluate their behavior in terms of corrosion and permeability.

In film metallizations were performed atomic force microscopy and electrochemical corrosion tests. In the electrochemical corrosion tests, film metallizations that only have zinc in their composition exhibited the best corrosion resistance. The film metallization with lower roughness has better electrical behavior compared with film metallization with higher roughness, which can explain the differences in the electrical behavior.

The metallizations were investigated in terms of permeability, adhesion to the cell and thermal conductivity. The Zn-SnCu₃ is the metallization that exhibits better adhesion to the cell, and consequently, better mechanical properties and lower oxide content. Additionally, SnZn is the metallization with lower value of thermal conductivity, which means that it is the best thermal barrier compared with the others metallizations. Finally, the metallization that exhibited lowest permeability and thus better cell protection against humidity, was the ZnAl (275 µm)-SnCu₃ (325 µm), due to the lower particle size and optimum condition of thickness to produce denser metallizations.

Keywords: Film capacitors, Biased 85°C/85% RH test, Flame spray, Arc spray, Permeability.

RESUMO

Vishay Intertechnology Inc. é uma empresa multinacional no sector dos componentes eletrónicos. É um produtor de semicondutores discretos e componentes eletrónicos passivos. Vishay Electrónica Portugal Lda em Vila Nova de Famalicão produz condensadores de filme, sendo estes o principal foco deste trabalho. Os condensadores de filme são aplicados em vários equipamentos eletrónicos e o seu correto funcionamento tem um grande impacto na fiabilidade e nos custos de manutenção de todo o sistema. Para testar a fiabilidade dos condensadores é utilizado o teste de tendência 85°C/85% HR. Neste teste, os componentes são expostos a 85°C e 85% humidade relativa durante 1000 horas. Deste modo, é necessário melhorar a construção do condensador e o seu desempenho.

Um condensador de filme é maioritariamente constituído por cinco partes: fita metalizada, metalização, terminais, resina isolante e copo. No decorrer deste trabalho, a fita metalizada e a metalização aplicada no topo da bobina foram testadas com o objetivo de avaliar o seu comportamento em termos de corrosão e permeabilidade.

As fitas metalizadas foram testadas por microscopia de força atómica e por testes de corrosão eletroquímicos. Nos testes de corrosão electroquímicos, as fitas metalizadas que só possuíam zinco na sua composição exibiram a melhor resistência à corrosão. A fita metalizada da Steiner tem o menor valor de rugosidade, o que explica o melhor comportamento elétrico comparando com a fita metalizada da Dhruv.

As metalizações foram investigadas em termos de permeabilidade, adesão à bobina e condutividade térmica. A metalização Zn-SnCu₃ é a que exhibe melhor adesão à bobina e, conseqüentemente, melhores propriedades mecânicas e menor teor de óxidos. Adicionalmente, SnZn é a metalização com menor valor de condutividade térmica, o que significa que é uma melhor barreira térmica comparando com as outras metalizações. Finalmente, a metalização que exibiu menor valor de permeabilidade e assim, melhor proteção da bobina contra a humidade, foi ZnAl (275 µm)-SnCu₃ (325 µm), devido ao menor tamanho da partícula e à condição ótima de espessura para produzir metalizações mais densas.

Palavras-chave: Condensadores de filme, Teste de tendência 85°C/85% HR, Pulverização à chama, Pulverização a arco, Permeabilidade.

TABLE OF CONTENTS

ACKNOWLEDGMENTS	vii
ABSTRACT	ix
RESUMO	xi
LIST OF FIGURES.....	xv
LIST OF TABLES.....	xix
ABBREVIATIONS.....	xxi
NOMENCLATURE.....	xxiii
Motivation.....	1
Objectives.....	3
CHAPTER 1 - State of the art.....	5
1.1. Capacitors	5
1.1.1. Metallized film capacitors.....	6
1.1.2. Materials used in Vishay's metallized film capacitors	12
1.2. Thermal Spray	15
1.2.1. Coating properties.....	20
1.2.2. Comparison between flame and arc spray	22
1.3. Temperature humidity bias test.....	23
CHAPTER 2 - Experimental Methodologies	25
2.1. Film metallizations	25
2.1.1. Winding	26
2.1.2. Electrochemical corrosion tests	27
2.1.3. Atomic force microscopy.....	28
2.1.4. Energy Dispersive X-ray Spectroscopy (EDS)	29
2.2. Metallizations.....	30
2.2.1. Flame and arc spray	31
2.2.2. Measurement of in-flight particles.....	33
2.2.3. Standard test method for water vapor transmission of materials	34
2.2.4. Scratch test	36
2.2.5. Thermal conductivity.....	37

CHAPTER 3 - Results and discussion	41
3.1. Film metallizations.....	41
3.1.1. Electrochemical corrosion tests.....	41
3.1.2. Atomic force microscopy.....	45
3.2. Metallizations	47
3.2.1. Measurement of in-flight particles.....	47
3.2.2. Porosity.....	48
3.2.3. Permeability	53
3.2.4. Scratch test.....	55
3.2.5. Thermal conductivity.....	57
CHAPTER 4 - Conclusions	61
4.1. Conclusions.....	61
4.2. Future works	63
REFERENCES	65

LIST OF FIGURES

Figure 1.1 – Five main stages in production of metallized film capacitors: a) Winding; b) Pressing; c) Metal spray; d) Welding or soldering; e) Final packing [17].....	7
Figure 1.2 – Equivalent circuit of a capacitor: ESR is the equivalent series resistance, C the capacitance and L the inductance [20].....	7
Figure 1.3 – Schematic of the capacitance parameters [8].	8
Figure 1.4 – Capacitance values for some capacitor types [8].....	9
Figure 1.5 – Representation of the dissipation factor [16].....	9
Figure 1.6 – Dissipation factors for several common capacitor dielectrics [8].	10
Figure 1.7 – Range of values for insulation resistance for some capacitor types [8].	11
Figure 1.8 – Schematic of the structure of a metallized film capacitor 1) Plastic case; 2) Insulating resin; 3) Metallization on top of the cell; 4) Film metallization; 5) Terminals.....	12
Figure 1.9 – Schematic view for flame spray [34].....	16
Figure 1.10 - Schematic view for arc spray [41].....	18
Figure 2.1 – Film metallizations (Vishay).	25
Figure 2.2 – 1848 film capacitor [48].	26
Figure 2.3 – Cell with the designation of the three parts (Vishay).	26
Figure 2.4 – Three-electrode experimental electrochemical cell (Dept. Physics, Univ. Minho).	28
Figure 2.5 – Atomic force microscopy equipment (Labmat, University of Minho).	29
Figure 2.6 - Energy dispersive X-ray spectroscopy equipment (SEMAT-UM, Guimarães) [54].	30
Figure 2.7 – Cell with the metallizations applied and the terminals.	30
Figure 2.8 – Plastic cases with grid to obtain the particles before the impact.	33
Figure 2.9 – Plastic cases in the substrate of the spraying machine (Vishay).	33
Figure 2.10 – a) and b) water filtration of the particles.....	34
Figure 2.11 – Test dishes with the samples attached.	35

Figure 2.12 – a) Weight of the test dishes (Vishay); b) Climatic chamber (Vishay).	36
Figure 2.13 – Scratch test equipment (SEMAT-UM Guimarães) [60].	37
Figure 2.14 - HMS-5300 Hall Effect Measurement System (Dept. Physics, Univ. Minho).	38
Figure 2.15 – Test assembly for thermal conductivity measurements: 1) Digital thermometer; 2) Multimeter; 3) Software; 4) Power supply; 5) Micro size infrared optical pyrometer; 6) Pt100 sensor; 7) Sample (Dept. Physics, Univ. Minho).	39
Figure 3.1 - Open circuit potential evolution with time for F1, F2, F3 and F4 film metallizations.	41
Figure 3.2 - Potentiodynamic polarization curves for F1, F2, F3 and F4 film metallizations.	42
Figure 3.3 – EDS results for a) F1, b) F2, c) F3 and d) F4 film metallizations.	43
Figure 3.4 – Open circuit potential evolution with time for F5 and F6 film metallizations.	44
Figure 3.5 – Potentiodynamic polarization curves for F5 and F6 film metallizations.	44
Figure 3.6 – 3-D view of superficial topography of a) F5 film metallization and b) F6 film metallization.	45
Figure 3.7 - 2-D view of superficial topography of a) F5 film metallization and b) F6 film metallization.	46
Figure 3.8 – Average roughness comparison between F5 and F6 film metallizations.	46
Figure 3.9 – Optical micrographs of particles for a) Sn-Cu ₃ ; b) Sn-Zn ₃₀ ; c) Zn; d) Zn-Al ₁₅ and e) Al.	47
Figure 3.10 – Values of particle size average for Sn-Cu ₃ , Sn-Zn ₃₀ , Zn, Zn-Al ₁₅ and Al.	48
Figure 3.11 – Comparison of the porosity between: a) Al - SnCu ₃ , b) Zn – Sn-Cu ₃ , c) Zn (electric arc) – Sn-Zn ₃₀ , d) Zn – Sn-Zn ₃₀ , e) Zn-Al ₁₅ – Sn-Cu ₃ and f) Zn-Al ₁₅ – Sn-Zn ₃₀ samples.	49
Figure 3.12 – Optical micrographs of a) Al – Sn-Cu ₃ ; b) Zn – Sn-Cu ₃ ; c) Zn (electric arc) – Sn-Zn ₃₀ ; d) Zn – Sn-Zn ₃₀ ; e) Zn-Al ₁₅ – Sn-Cu ₃ and f) Zn-Al ₁₅ – Sn-Zn ₃₀	50
Figure 3.13 - Porosity comparison between the samples with different thicknesses produced by ABM machine.	51
Figure 3.14 – Optical micrographs of a) Zn ABM (225 μm) and b) Zn ABM (800 μm).	51

Figure 3.15 – Porosity comparison of the Zn-Al15 - SnCu3 samples with different thicknesses.	52
Figure 3.16 – Optical micrographs of a) Zn-Al15 (225 μm) – Sn-Cu3 (225 μm); b) Zn-Al15 (325 μm) - Sn-Cu3 (325 μm); c) Zn-Al15 (225 μm) – Sn-Cu3 (145 μm); d) Zn-Al15 (275 μm) – Sn-Cu3 (325 μm).....	52
Figure 3.17 - Permeability values for Zn-Al15, Sn-Cu3, Zn and Sn-Zn30.	53
Figure 3.18 - Permeability values for Zn ABM (225 μm) and Zn ABM (800 μm).	54
Figure 3.19 - Permeability values for a) Zn-Al15 (225 μm) – Sn-Cu3 (145 μm), b) Zn-Al15 (275 μm) – Sn-Cu3 (325 μm), c) Zn-Al15 (225 μm) – Sn-Cu3 (225 μm) and d) Zn-Al15 (325 μm) – Sn-Cu3 (325 μm).....	55
Figure 3.20 - Tested samples (Zn-Al15 – Sn-Cu3) with and without the scratches.....	55
Figure 3.21 – Scratch test results for Zn-Al15 – Sn-Cu3.	56
Figure 3.22 – Optical micrograph of the scratch for Zn-Al15 – Sn-Cu3 sample a) Initiation of the cracks; b) Final spallation failure.	56
Figure 3.23 – Electrical conductivity evolution with temperature of Sn-Zn30, Sn-Cu3, Zn, Zn-Al15, Zn ABM 225 μm and Zn ABM 800 μm	58
Figure 3.24 - Thermal conductivity at two different temperatures for Sn-Zn30, Sn-Cu3, Zn, Zn-Al15, Zn ABM 225 μm and Zn ABM 800.	59

LIST OF TABLES

Table 1.1 – Materials used in the production of Vishay metallized film capacitors.....	12
Table 1.2 – Properties of the dielectrics [20].	13
Table 1.3 - Wider comparison between flame and arc spray [30].	22
Table 1.4 - Comparison of costs between flame and arc spray [19].	22
Table 2.1 – Designation with the reference, the supplier and the dimensions of the four types of film metallizations.	25
Table 2.2 - Designation with the reference, the supplier and the dimensions of the two types of film metallizations.	25
Table 2.3 – Parameters used in winding of the film metallizations.	27
Table 2.4 – Materials properties used in the five metallizations types [55]–[58].	31
Table 2.5 – Comparison between the flame spray parameters used in Vishay and those mentioned in the literature [30], [33].	32
Table 2.6 - Comparison between the arc spray parameters used in Vishay and those mentioned in the literature [30], [33], [38].	32
Table 2.7 – Samples with the thicknesses and the method that were tested.	35
Table 2.8 – Samples tested in scratch test with thickness of 500 μm	37
Table 3.1 - E_{corr} and i_{corr} for F1, F2, F3 and F4 film metallizations.	42
Table 3.2 – Quantification by EDS for the four film metallizations.....	43
Table 3.3 – E_{corr} and i_{corr} for F5 and F6 film metallizations.....	45
Table 3.4 – Roughness average (Ra) for F5 and F6 film metallizations.....	46
Table 3.5 – Values of particle size average for Sn-Cu3, Sn-Zn30, Zn, Zn-Al15 and Al.	47
Table 3.6 – Porosity values for all tested samples.	49
Table 3.7 – Permeability average values for all tested samples.	53
Table 3.8 - Results of the failure initiation and critical adhesion failure load, relative to scratch length.....	57
Table 3.9 – Electrical conductivity results at 77 $^{\circ}\text{C}$	58

Table 3.10 - Thermal conductivity values of Sn-Zn30, Sn-Cu3, Zn, Zn-Al15, Zn ABM 225 μm
and Zn ABM 800. 59

ABBREVIATIONS

2D	Two dimensional
3D	Three dimensional
AC	Alternating current
AE	Acoustic emission
AFM	Atomic force microscopy
C/CL	Closed nozzle with green cap and converging orifice
CD/CL	Closed nozzle with a converging-diverging orifice
CD/OP	Open nozzle with a converging-diverging orifice
CTE	Coefficient of thermal expansion
DC	Direct current
E_{corr}	Corrosion potential
EDS	Energy dispersive X-ray spectroscopy
GF	Glass fiber
HVOF	High velocity oxygen fuel
i_{corr}	Corrosion current density
ICs	Integrated circuits
MKP	Metallized polypropylene film
MKT	Metallized polyester film
MMCs	Metal matrix composites
MOSFETs	Metal oxide semiconductor field effect transistors
OCP	Open circuit potential
OM	Optical microscope
PBT	Polybutylene terephthalate
P_c	Critical load
PD	Potentiodynamic polarization
PPS	Poly (p-phenylene sulfide)
RH	Relative humidity
SCE	Saturated calomel electrode
SEM	Scanning electron microscopy
WVT	Water vapor transmission

NOMENCLATURE

A	Area
C	Capacitance
d	Distance
ESR	Equivalent series resistance
I_{leak}	Leakage current
k	Thermal conductivity
L_z	Lorenz factor
L	Inductance
N	Number of sample points evaluated
q	Charge
Ra	Roughness average
R_{is}	Insulation resistance
r_i	Absolute value of the roughness
$\tan \delta$	Dissipation factor
T_{intern}	Temperature of the Pt100 sensor
U_{dc}	Applied DC voltage
V	Voltage
X_c	Capacitive reactance
ϵ_0	Permittivity of vacuum
σ	Electrical conductivity

Motivation

Vishay Intertechnology Inc. is a worldwide company in electronic components sector. It is a manufacturer of discrete semiconductors and passive electronic components and its portfolio includes semiconductors (MOSFETs, integrated circuits (ICs), rectifiers, modules, diodes and thyristors and optoelectronics) and passive components (resistors, inductors and capacitors) [1].

Vishay Electrónica Portugal Lda in Vila Nova de Famalicão produces film capacitors, which will be the main focus of this work.

Film capacitors consist of two metallic plates electrodes that are separated by an insulating film such as polyester or polypropylene, named dielectric [2], [3]. Comparing with other capacitor types, film capacitors are known to have lower heat dissipation and longer lifetime [4]. In metallized film capacitors, the electrodes consist in a thin metal layer with a thickness of several tens of nanometers that is deposited under vacuum conditions. The electrodes are then rolled in a cell and the end-faces are metal sprayed by flame or arc spray in order to provide electrical contact to the terminals, which are connected to the end-faces by welding or soldering. The cell is then sealed in a plastic case where resin is deposited into the plastic case [2], [3]. This type of capacitors have a high volume efficiency, self-healing properties, high energy-storage density and are highly reliable units [3], [5].

Film capacitors are applied on several electronic equipments in automotive and renewable energy industry, outdoor applications, telecommunications and consumer electronics. These industries require additional reliability for applications under very critical environmental conditions. The reliability of the capacitors has a major impact on the operational reliability and maintenance costs of the whole system [2]. Due to that, there are several tests that the capacitor industry frequently uses to test the reliability of the components. Biased 85°C/85% RH test is the most critical test for the qualification of the capacitors. In this test, the components are exposed at 85°C and 85% relative humidity during 1000 hours. Nowadays, many customers require this test as a specification of the capacitor [6]. However, there are few producers that ensure that the capacitors pass the aforementioned biased 85°C/85% RH test.

Vishay Electrónica Portugal Lda wants to ensure their customers that the capacitors pass the biased 85°C/85% RH test. In this way, it is necessary to improve the capacitor construction acting in the metallization used on top of the cell, in the film metallization or in the resin and the plastic case. In this work, the film metallization and the metallization applied on top of the cell will be studied.

Objectives

The main objective of this work is to study the tightness of the metallization used on top of the thin film capacitor cell. It is expected that the better the tightness of the metallization, the better the tightness of the thin film capacitor cell and the better the chances to the capacitor passes the biased 85°C/85% RH test. In this way, it is necessary study the materials of the metallization in terms of permeability. In order to accomplish this, there are several necessary steps, such as:

- Evaluate parameters such as the grain thickness, adhesion between the materials, presence of impurities, temperature and humidity.
- Determine the most suitable material to protect the cell against corrosion and humidity.
- Verify if the particle size and thickness affects the permeability of the metallization.
- Study the film metallization.
- Study the differences between flame and arc spray.
- Search for new processes and solutions.

CHAPTER 1 - State of the art

1.1. Capacitors

A capacitor is a passive electronic component, essential in circuit boards, which will accumulate a charge when is connected through a DC/AC power source. In this way, as the capacitor has the capability to store energy and then discharge it, it will act as a small rechargeable battery. Capacitors have advantages over the batteries, such as: not contain harmful metals (lead, for example) which will do not cause environmental issues and have higher charge and discharge cycles with higher speed. A capacitor can also be used to smooth the output voltage provided by power supplies [7]–[9]. The reliability of these components has a major impact on the reliability and maintenance costs of the entire system [5].

In its simplest form, a capacitor consists in two parallel metallic plates (electrodes), with an insulating between, each with a connection attached to a DC/AC power source. The electrons will migrate to the plate attached on the negative side of the source and will repel the electrons from the plate attached on the positive side. The capacitor charges through moving the electrons from the power source between the plates. The resultant electrical energy is stored in the polarized insulating medium, although this energy will gradually dissipate as a result of the leakage due to the insulating medium. This electrical energy can be stored over a long charging time and then released as required in short periods under controlled conditions [7], [10], [11]. The measured amount of stored energy is the capacitance. The value of the capacitance is directly proportional to the area of the electrodes and inversely proportional to the distance between the electrodes. In order to increase the capacitance of a capacitor, a thin insulating layer, known as the dielectric, is placed between the plates. The value of the capacitance is proportional to the dielectric constant of the insulator. The dielectric constant value for air is 1.00 and for polyester is 3.2, which means that for the same distance between the plates, polyester will have 3.2× the capacitance. The higher the value of the dielectric constant, the higher is the capacitance for the same given area and distance between the electrodes. Likewise, the dielectric layer determines the potential at which the capacitor breaks down [10], [12]. This dielectric can be ceramic, polymer or ceramic/polymer in a solid, gas or liquid state, gel or vacuum [7], [9]. Polymer dielectric compared with ceramic dielectric has good flexibility and performance, however has lower dielectric constant [9]. This polymer dielectric can be made of polyester, polypropylene, polycarbonate, polystyrene or

polyimide with thicknesses between 2 to 20 μm . The width of the polymer dielectric determines the inductance of the capacitor [12], [13]. The metallic plates in most capacitors are made from thin metallic plate deposited in the plastic film [7]. Both metallic plates are charged in opposite sides by a voltage source and the resultant electrical energy of this charged system is stored in the polarized insulating medium [11].

There are several capacitor types that are differentiated by the materials used in their construction such as ceramic disk capacitors, multilayer ceramic capacitors, film and foil capacitors, electrolytic capacitors and tantalum capacitors [8], [14]. The main focus of this work are the film capacitors and these type of capacitors can be subdivided into three construction types: film/foil capacitors, metallized film capacitors and mixed technology capacitors [13]. Among these three, the type that Vishay Electrónica Portugal Lda produces is the metallized film capacitor.

1.1.1. Metallized film capacitors

In metallized film capacitors, the metal layer in the polymer dielectric is typically aluminum, zinc or an alloy of aluminum-zinc and is very thin (in the range of 0.02 to 0.05 μm) that is previously vacuum deposited (by chemical or physical vapor deposition) directly on the dielectric substrate forming the film metallization. The production of a metallized film capacitor begins with the winding of alternating film metallization in order to form a cell. The tension in the film metallization is maintained to avoid the shrinkage or the breaking of the film and a pressure roller is used to avoid air gaps between them [5], [7], [12], [13], [15]. This type of capacitor has a free margin that is a small portion of the film metallization where there is no metal layer, in order to provide the electrical isolation between the two films during metal spraying. After winding, the cell is pressed in order to remove the air gap. Before the metal spray, a masking process is made with aim to cover the lateral faces with a tape to avoid the deposition of metal particles during spraying. Hereafter, the end faces are metal sprayed by arc or flame spray and this metallization provide electrical contact to the terminals. In order to obtain a good electrical contact, it is important that during the metal spray, the particles of metal fill all the gaps produced by the offset of winding films. When metal spray is completed, the cells undergo a thermal treatment (in order to stabilize the polymer dielectric), de-masking and de-burring (to remove the burrs formed in spraying process).The terminals are connected in the metallization used on top of the cell by welding or soldering. Subsequently, some cells are impregnated with wax, so that the epoxy will adhere effectively. Afterwards, the cell is set in a plastic case and surrounded by electrically insulating resins. This step must be carried out within 24 hours after metal spray, however it is better to be done immediately after metal spray to reduce any opportunity of moisture or pollutants penetrate in the

cell. The five main stages in production of the metallized film capacitors are presented in Figure 1.1 [3], [4], [15]–[19].

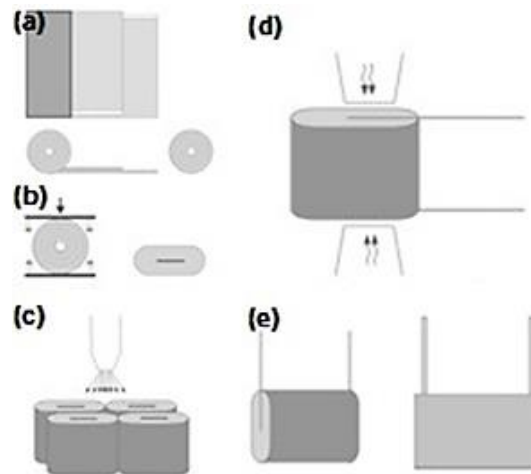


Figure 1.1 – Five main stages in production of metallized film capacitors: a) Winding; b) Pressing; c) Metal spray; d) Welding or soldering; e) Final packing [17].

Finally, the capacitors are electrically tested with the specified capacitance value, dissipation factor ($\tan \delta$) and insulation resistance (R_{is}).

i. Capacitance

Capacitance is the capacitive part of the equivalent circuit composed of capacitance, equivalent series resistance and inductance (Figure 1.2).

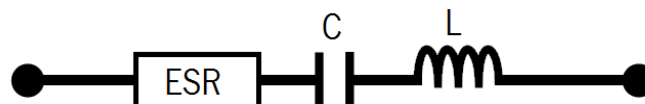


Figure 1.2 – Equivalent circuit of a capacitor: ESR is the equivalent series resistance, C the capacitance and L the inductance [20].

The capacitance (C) is the measure of the energy (charge) (q) that a capacitor is capable to storage at an applied voltage (V) [21]:

$$C = \frac{q}{V}$$

As a result of this equation, the value of capacitance is given as a unit, multiple or submultiple of the farad (F): one farad its equal to one coulomb (C) per 1 volt (V) and one coulomb represents 6.24×10^{18} electrons [8]. Capacitance depends on the geometry and composition of the capacitor. The value for which capacitor has been designed is named rated capacitance and is normally marked on the product. There is a tolerance in the capacitance value and is defined as the deviation of the capacitance from the rated

capacitance. Its measured in a free air ambient temperature of $23 \pm 1^\circ\text{C}$ and RH of $50 \pm 2\%$ [10], [20], [22].

In the simple parallel-plate capacitor, the capacitance is given by:

$$C = \frac{\epsilon_0 A}{d}$$

where $\epsilon_0=8.85 \times 10^{-12}$ F/m and is the permittivity of vacuum, d is the distance between the plates (in m) and A the plates area (in m^2). Figure 1.3 shows the capacitance parameters schematically [8].

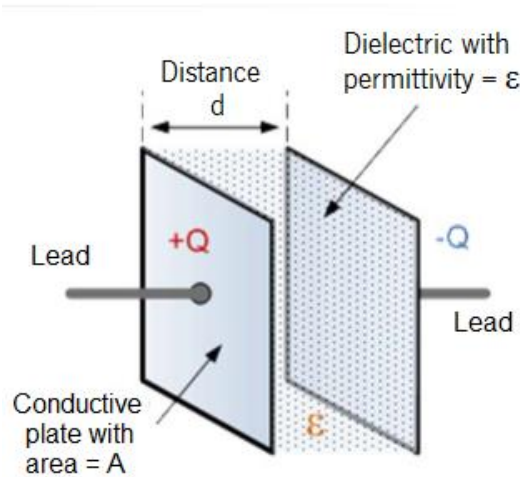


Figure 1.3 – Schematic of the capacitance parameters [8].

The majority of capacitors are a variation of this design, so, in order to increase the capacitance, it is necessary increase the area of the electrodes (metallic plates), decrease the distance between them or change the dielectric material for one with high dielectric constant [8], [10].

Taking into consideration several parameters such as the physical characteristics of the electrode plates, the distance between them and the dielectric constants, in Figure 1.4 is presented the range of capacitance values for some capacitor types [8].

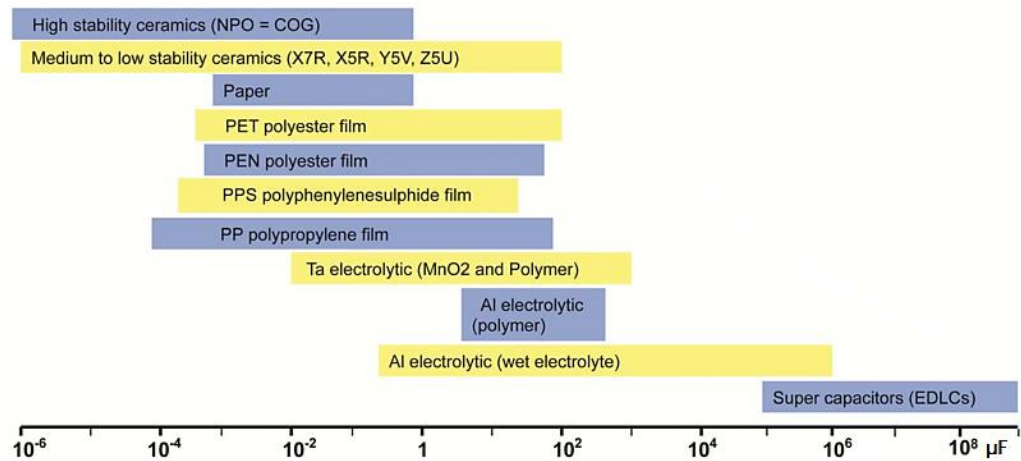


Figure 1.4 – Capacitance values for some capacitor types [8].

ii. Dissipation factor ($\tan \delta$)

The dissipation factor ($\tan \delta$ in %) is the loss in power of the capacitor divided by the reactive power of the capacitor at a sinusoidal voltage of specified frequency and is temperature and frequency dependent. An ideal capacitor has no dissipation. This value depends on the equivalent series resistance (ESR) and capacitive reactance (X_c) (Figure 1.5), and is given by [8], [16]:

$$\tan \delta = \frac{ESR}{X_c}$$

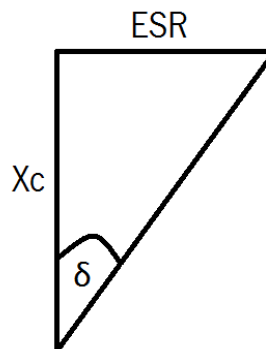


Figure 1.5 – Representation of the dissipation factor [16].

The dissipation factor value reflects the polarization losses of the dielectric film and the losses caused by the contact resistance between the terminals, the metallization and the film metallization. Parallel losses can occur due to the high insulation resistance of film capacitors and these losses sometimes are neglected. Figure 1.6 compares the dissipation factors for several common capacitor dielectrics [8], [16].

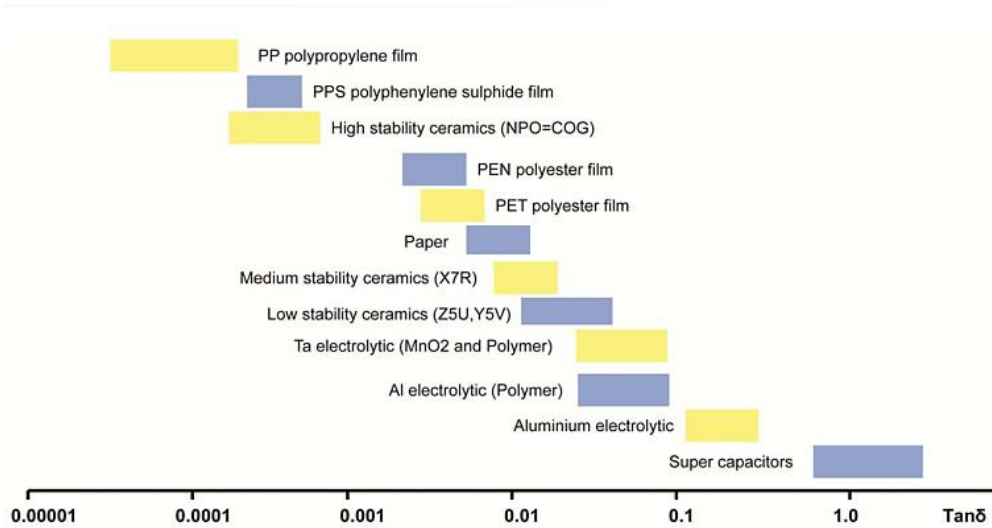


Figure 1.6 – Dissipation factors for several common capacitor dielectrics [8].

iii. Insulation resistance (R_{IS})

Insulation resistance (R_{IS}) is a measure of the ability of a non-conducting material resist to an electric current when a potential is applied and is defined as [23]:

$$R_{IS} = \frac{U_{pc}}{I_{Leak}}$$

where U_{pc} is an applied DC voltage and I_{Leak} is the leakage current. For practical reasons, insulation resistance can be expressed in mega ohms for low capacitance values and in ohm-farads for high capacitance values. The insulation resistance is determined by the quality and properties of the dielectric and the capacitor construction [8], [16]. Testing of this property is important for evaluate the leakage integrity between interconnections that are theoretically electrically isolated. In the case of metallized film capacitors, the two conductors are separated by the dielectric and the leakage will occur through the bulk of the insulating material (dielectric) [14].

If insulation resistance fails in metallized film capacitors, it means that there is a problem, such as, the degree of cure of the resins and the porosity or defects (voids and micro cracks) in the metallization. The purpose for the determination of the insulation resistance is to evaluate the reliability of the capacitors in regard to its operation in a humid environment. A high relative humidity will decrease the insulation resistance. In order to evaluate this property, a temperature humidity bias test is made in the metallized film capacitors. The range of values for insulation resistance for some capacitor types is shown in Figure 1.7 [8], [14], [16].

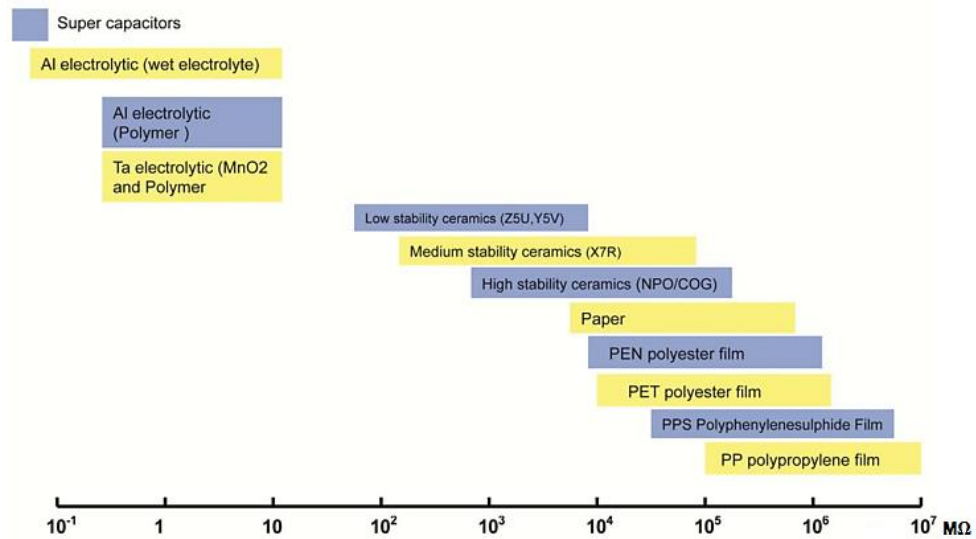


Figure 1.7 – Range of values for insulation resistance for some capacitor types [8].

Metallized film capacitors are characterized by their low cost, small size and the capability to undergo “self-healing”. These capacitors have a high energy-storage density (<3 kJ/L) and are considered high-reliable units and, due to that, are used in applications that requires a wide range of operating temperatures, high pulse current rating and a wide range of operating frequencies. However, these capacitors types have low insulation resistance [3], [5], [13], [15], [18], [24]–[26].

Self-healing is a property exclusive of the metallized film capacitors being the principal advantage over film/foil capacitors. When voltage is sufficient to break down the dielectric, the electrodes are exposed to each other. A small portion of the stored energy in the capacitor discharges into the short, creating a heated area that will vaporize the metal away from the break down (pin hole). The arc will be extinct and the metal will be oxidized and redistributed, resulting in a clearing area without metal around the breakdown site. The metallized film capacitor repairs itself, due to the thin thickness of the films used and the high energy density at the fault area and the capacitor stays in operation. This recovery is influenced by the thickness of the electrode, the capacitance value and the applied voltage. During self-healing, only a fraction of the energy stored in the capacitor is dissipated. The only permanent change is the loss of a small amount of capacitance. This allows the use of the dielectric for higher stress without failure. In other hand, in a film/foil capacitor, when the foils are exposed to each other, the foils will touch and short together which will make the capacitor useless [5], [12], [13], [24].

The performance of these capacitors deteriorates continuously over time due to operational factors such as voltage, current reversal, temperature, pulse repetition rate, stressed area. This degradation is gradual: initially takes place a soft degradation, while total failure rarely occurs. When the loss of capacitance is under a critical level, the performance of capacitors remains stable.

However, when the loss of capacitance goes beyond that critical level, the performance of capacitors starts to decrease and the degradation rate of the dielectric and the rate of capacitance loss increase quickly. End of life for metallized film capacitors is defined as loss of a specified amount of capacitance, typically 5% [5], [26].

1.1.2. Materials used in Vishay's metallized film capacitors

In Figure 1.8 is presented a schematic of the structure of a metallized film capacitor produced in Vishay Electrónica Portugal Lda.

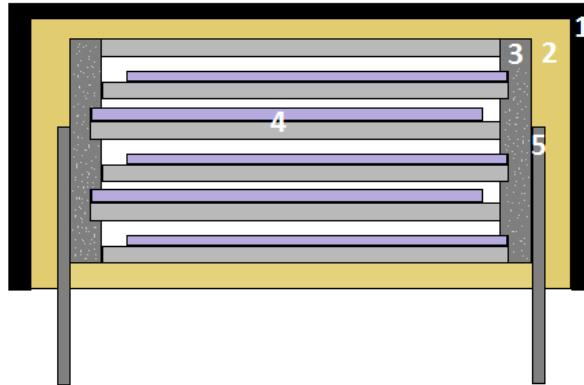


Figure 1.8 – Schematic of the structure of a metallized film capacitor 1) Plastic case; 2) Insulating resin; 3) Metallization on top of the cell; 4) Film metallization; 5) Terminals.

The materials used in the production of Vishay metallized film capacitors are presented in Table 1.1.

Table 1.1 – Materials used in the production of Vishay metallized film capacitors.

Component	Materials
1) Plastic case	Poly(p-phenylene sulfide) (PPS) or Polybutylene terephthalate with 15% glass fiber (PBT 15% GF)
2) Insulating resin	V80, V81 or V70 (Epoxy resins)
3) Metallization on top of the cell	Zinc (Zn), Zinc-Aluminum (Zn-Al15), Aluminum(Al), Tin-Copper (Sn-Cu3) or Tin-Zinc (Sn-Zn30)
4) Film metallization	Metallized polyester film (MKT) or Metallized polypropylene film (MKP) with Zinc-Aluminum (Zn-Al) or Aluminum (Al)
5) Terminals	Tinned copper

Since the focus of this work is the film metallization and the metallization used on top of the thin film capacitor cell, in the next topics it will be described these components.

- **Film metallization**

The materials of the film metallization usually are polyester or polypropylene film metallized with zinc-aluminum or aluminum. These two dielectrics have different properties (Table 1.2).

Table 1.2 – Properties of the dielectrics [20].

Parameter	Dielectric	
	Polyester (KT)	Polypropylene (KP)
Dielectric constant at 1 kHz	3.3	2.2
Dissipation factor at 1kHz (10^{-4})	50	1
Volume resistivity ($\Omega \cdot \text{cm}$)	10^{17}	10^{18}
Dielectric strength ($\text{V}/\mu\text{m}$)	400	600
Maximum application temperature ($^{\circ}\text{C}$)	125	105
Power density at 10kHz (W/cm^3)	50	0.6
Dielectric absorption (%)	0.2	0.01

Polyester films are mostly used in general capacitors and are widely used in DC applications. This dielectric is available in a wide range of thicknesses, ranging from 0.5 to 20 μm . Combining the thin film with relatively high dielectric constant, high energy densities are possible. The most important property is its high capacitance per volume due to its high dielectric constant and availability in thin gages. However, polyester film has high dissipation factor which increases with temperature and frequency, and is typically used in applications with small bias DC voltage and small AC voltages at low frequencies. On the other hand, polypropylene films are available in thicknesses ranging from 3 to 15 μm and have superior electrical characteristics. This dielectric has advantages such as high breakdown strength, low moisture absorption, low dissipation factors and capacitance stability throughout the temperature range. It is ideally suited for high frequency and high current applications. Due to that, are used in AC, pulse and interference suppression capacitors for main applications. The disadvantages are the relatively low dielectric constant compared with polyester films and its low maximum application temperature [3], [7], [12], [20], [27].

- **Metallization used on top of the thin film capacitor cell**

The metallization used on top of the thin film capacitor cell is extremely important in a capacitor. As mentioned before, this metallization provides the electrical contact for the terminals. The capacitor tightness is equally important, since it is expected that the better the tightness of the metallization, the better the tightness of the cell. Nevertheless, it is important to study the electrical behavior with the variation of the tightness.

In Vishay capacitors, the metallization has two layers, both with thickness around 225 μm : the first layer can be Zinc (Zn), Aluminum (Al) or Zinc-Aluminum (Zn-Al15) and the second Tin-Copper (Sn-Cu3) or Tin-Zinc (Sn-Zn30). The materials combination for the layers depends on the capacitor type. The use of tin in the second layer is necessary for soldering with several solder alloys. Zinc is more difficult to solder and requires the use of specific solder compositions and owing to that is not applied in the second layer. Due to the higher melting point compared with the material of the dielectric, shrinkage in the film metallization can occur, depending on the zinc droplet dimension and this reduces the effective surface of contact, decreasing the mechanical durability of the electrical contact. However, zinc is widely used due to its high adhesion strength and low heat capacity, which makes it proper for the first layer [18], [25].

1.2. Thermal Spray

Thermal spray is a general term for a group of coatings processes with the aim to apply metallic and nonmetallic coatings in order to improve or restore the surface of a solid material [28]. This technology is used since 1900s, however recent developments in process and equipment have improved the quality of the coatings and expanded their range of applications [19], [29]. This technology is used in applications for wear and erosion resistance, dimensional restoration and repair, thermal insulation and control, electrical resistance and conductivity, corrosion and chemical resistance, oxidation resistance, biomedical compatibility and many other applications [28], [30]. It has been widely used to extend the life of new components or repair and reengineer damaged components, and normally leads to costs saving in terms of production and maintenance. A few common applications are: road vehicles, ships, aircraft, electric motors, valves, power generation and aerospace turbine repair, pumps, gate and ball valves, aerospace combustion chambers and electrical industry [19], [28].

There are several types of thermal spray processes, such as [28], [31]:

- Flame spray;
- Powder spray;
- Arc spray;
- Plasma spray;
- High velocity oxygen fuel (HVOF) spray.

These techniques are metallurgical cold processes and use different energy sources to molten or semi molten the coating material (in powder or wire). The molten or semi molten particles are then accelerated and forced onto a cleaned and prepared surface by process gases or atomization jets. Upon impact, from the combined thermal and kinetic energy, the particles form bonds with the surface and with the subsequent particles, in order to produce a cohesive coating of successive layers with lamellar structure. These particles experience very high cooling rates, typically 10^6 K/s for metals. Coatings can have thicknesses from 100 to 750 μm . The major advantages of these thermal spray processes are the wide range of materials that can be used to produce coatings (theoretically, any material without decomposing can be used) and the capability to apply coatings without significant heat input. Thermal spray coatings have several characteristics that are attractive for different types of industries, but for capacitor manufacturers, the heat resistance (thermal barrier coating), corrosion and oxidation resistance and good electrical conductivity are the most important characteristics [28], [30], [32]. Vishay uses flame spray and arc spray to apply the metallization on top of the thin film capacitor cell.

1. Flame spray

Conventional flame spray was the first type of thermal spray developed in 1917 and it still is vastly applied in current industries. Flame spray uses the chemical energy of the combustion of the fuel gases (acetylene or propane) to generate heat to melt the end of the wire. The feedstock material (wire) is introduced axially through the nozzle into the flame to be melted, and a stream of air atomizes the molten particles and propels them onto the surface. The driving of the wire is made by an air motor with a gearbox that is part of the gun body (Figure 1.9) [30], [31], [33].

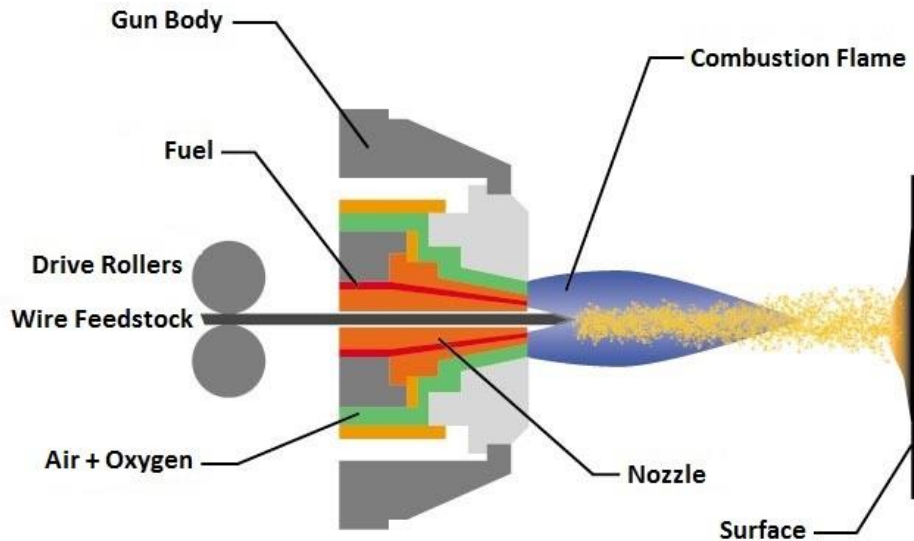


Figure 1.9 – Schematic view for flame spray [34].

The total gas flow, the wire feed rate and standoff distance are adjusted to produce the desired properties of the metallization. With this process, it is possible to deposit a wide range of materials such as polymers, ceramics and refractory metals. The resulting coating of this process has densities ranging from 85 to 98%, depending on the coating material and particular technique. In the microstructure of the resulting coating it is common to find the presence of oxide inclusions and porosity [30], [33]. In flame spray, increasing the power levels and the spray distance will lead to an increase in coating porosity and tensile strength. The thickness of the coating is related to the feedstock rate impacting the substrate per time unit: this value depends on the torch-substrate relative velocity, the scanning step, the standoff distance and the power feed rate. The thickness of the coating is maximal for low velocity and scanning step combined with a high feedstock weight rate [35].

In respect of health and safety issues, care must be taken with the flammable gases, the production of dust and the high production of noise. The excessive exposure to these factors can be hazardous for the operator [31], [36].

There are several works that investigated the influence of the operating parameters in the flame spray. For example, Huonnic et al. [37] investigated the feasibility of flame sprayed deposition of a thin coating of aluminum on cured basalt and glass fiber reinforced epoxy matrix composites with limitation degradation of the composite. They quantified the quality of the coating with electrical resistance measurements, characterized the microstructure and the thickness of the coating and investigated the possible effects of degradation due to the grit blasting and flame spraying processes through mechanical pressure testing. In flame spray, the standoff distance used was 150 mm, the torch was moved linearly across the composite tube at 75 mm/s, while the tube was rotated at 120 rpm. The flame spray combustion gas mixture was acetylene at 15 l/min and oxygen at 25 l/min. They conclude that, by using appropriated flame spray parameters, a coating could be produced onto the polymer surface without any visible significant distortion and deterioration of the substrate. Mild grit blasting was made to promote the adhesion to the substrate and without this step, the metal coating did not adhere to the surface and is easily removed.

2. Arc spray

The arc spray process was developed in approximately 1910, but only in the 1960s did this process gain commercial approval. The market demands for advanced applications leads to efforts toward a better understanding of the process fundamentals in order to develop more sophisticated control techniques to improve the coating quality and the productivity. Arc spray is commonly used and is an inexpensive thermal spray technique, where the material to be deposited is introduced into the gun as wires in the form of consumable arc electrodes. One advantage of this method is the possibility to produce a pseudo-alloy coating since the used wires can be of different materials. The resulting coatings are typically denser and stronger than their equivalent combustion spray coatings. Due to the low running costs, high spray rates and efficiency, arc spray is a good process for spraying large areas. Also, it is possible to spray a widespread range of metals, alloys and metal matrix composites (MMCs) with a broad range of thicknesses, since thick coatings for plastic injection moulding to thin coatings for circuit boards. Arc sprayed coatings are used typically to fight both high and low temperature corrosion. Furthermore, these coatings offer excellent resistance to atmospheric corrosion and can be used on bridges and other infrastructure components. In the same way, several aircraft engine manufacturers specify the use of the arc spray technique for repairs of many aircraft engine components, such as dimensional restoration and hot temperature erosion resistance, for example [29], [38], [39].

In arc spray deposition, two wire electrodes, connected to a high direct current (DC) power source, are fed into the gun by an air or electric motor and gearbox arrangement, and a high voltage electric arc (similar to a welding arc) is formed in the gap between the wires, heating them. The ends of the wires are molten and then dispersed and propelled by a gas stream (air or nitrogen) onto the surface. A secondary gas stream can be used for further atomization and is injected after primary atomization. After impact, the particles deform and solidify in order to build up a coating (Figure 1.10) [25], [29]–[31], [33], [40].

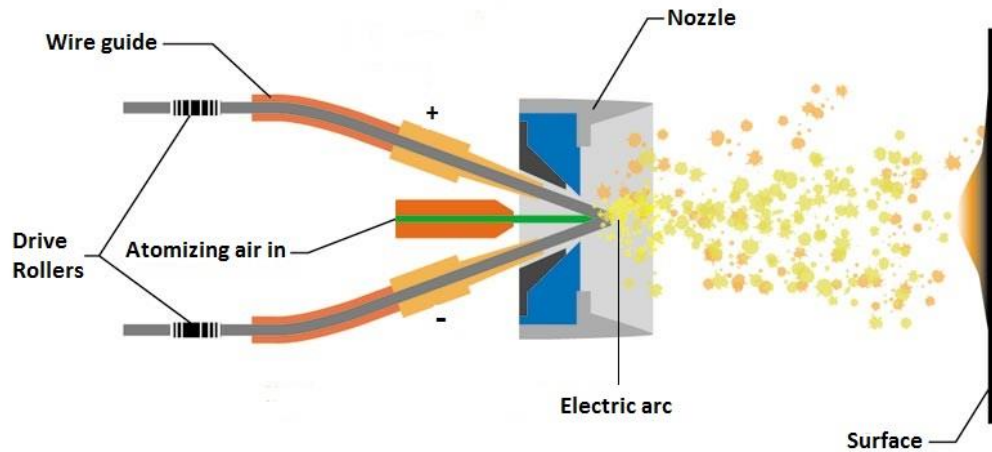


Figure 1.10 - Schematic view for arc spray [41].

The temperature in the arc can reach 5500°C , and the particles velocities are in the range of 100-300 m/s. Due to the high temperature of the arc and particle velocity, arc sprayed coatings have higher bond strength and lower porosity levels comparing with flame sprayed coatings. However, these coatings have higher oxide content due to the use of compressed air for droplet atomization and propulsion, which will oxidize the molten material [29].

In particular, the particles are molten when entering the air stream and begin to cool immediately after leaving the electric arc, which does not occur in other processes. Moreover, thermal efficiency of this process is higher comparing to other thermal spray processes due to the direct melting of wires by the arc. Although, in the literature it has been found that during wire arc spraying the arcing and melting of the tips is unstable. The wire melting rate is not equal, resulting in a periodic variation of arc length and arc voltage. This results in a periodic variation of the molten droplet size that leads to a bimodal particle size distribution, with smaller particles being related to the cathode. Therefore, this will influence the coating properties, such as porosity and oxide content. This process is simple, can be operated manually or in an automated manner and can be carried out using inert gases or a controlled atmosphere chamber. The heat transfer per particle to the substrate is lower than in other thermal spray processes, due to the absence of a flame or

plasma. This enables the deposition of coatings onto polymers, fiberglass, wood and paper as well in metallic or glass substrates. Additionally, the size and distribution of particles are a function of the operating parameters. For example, the particle size increase is due to: an electric current increase, a voltage decrease, a decrease in air flow or wire size increase. An increase in the arc current leads to an increasing frequency which results in an increase in the wire feed rate [30], [33], [40], [42]–[44].

In this case, one should also take care over health and safety issues due to the high production of noise and dust. On the other hand, due to an arc formation between the wires, the operator's eyes must be protected by a darkened visor of a suitable grade. The excessive exposure to these factors can be hazardous for the operator [31], [36].

There are several works that are dedicated to understand the droplet formation, in flight particle properties such as particle size, temperature and velocity, and the effects of spray parameters such as nozzle configuration and atomizing gas pressure since they contribute to coating properties [42].

For example, Liao et al. [42] studied the effect of particles properties from individual wires, using as anode and cathode, two consumable wires with different magnetic properties and the effect of the nozzle geometry. They studied three different nozzle shapes: the standard TAFE 9000 spray nozzle that corresponds to a closed nozzle with green cap and converging orifice (C/CL), a closed nozzle with a converging-diverging orifice (CD/CL) and an open nozzle with a converging-diverging orifice (CD/OP). The two wires used were steel and copper with 1.6 mm diameter. They collected the particles after spraying onto water with a standoff distance of 300 mm, an arc current of 200 A and an arc voltage of 30 V. They found a bimodal particle size distribution. The CD/CL nozzle produced the smallest particles and the CD/OP nozzle the largest ones. This difference becomes smaller when increasing the atomizing gas pressure or when using a CD/CL nozzle. In other hand, the CD/OP nozzle exhibits the coarsest microstructure due to the poor atomization and lower particle velocities. Large particles with low velocity and temperature will result in poor deformation and caking upon impact on the substrate, and due to that, they found many inter laminar cracks that implies poor bonding between the flattened particles and a lower cohesive strength. In other hand, they found a fine microstructure with lower porosity and higher oxide content using a CD/CL nozzle revealing a better atomization with higher particles velocities. They increased the arc current from 150 A to 200 A and conclude that this increasing leads to a reduced coating porosity. With higher arc current, droplets have higher temperature and lower oxidation

due to the increase of the wire feed rate, hence deform and calk more readily upon impact with rough surface.

1.2.1. Coating properties

The sprayed coating is built up particle by particle. The individual particle formation has a significant effect on the coating structure and properties. The air flow rate and the standoff distance are the two main parameters that affect the properties of the particles and therefore its impact on the substrate. The deposition of an individual particle forms a splat due to the process of impacting, flattening, rapid cooling and solidification. The degree of the splat formation is influenced by the droplet size, density, viscosity and impact velocity [38].

Using a high standoff distance could produce more porous coating due to the cooling and low velocity of the particles that are projected on the substrate. As a consequence, the deposition efficiency decreases. On the other hand, low standoff distances may lead to poor coverage on the coating due to the overheating of the particles and will produce internal thermal stresses. Hence, it is necessary find an optimum value of standoff distance to produce an optimal coating adhesion to the substrate. The angle of the spray nozzle must be perpendicular to the substrate for a better coating quality [19], [40].

A higher pressure and rate of the atomizing air results in higher impact velocity and gas stream, which will break up the molten particles into smaller droplets. This atomizing air is commonly used in wire and flame spray techniques. The major advantages are the availability and economy of compressed air. Smaller droplets will react more with oxygen compared with larger droplets due to their greater specific surface area. Oxide content increases with the increasing of the standoff distance. Mainly in arc spray, the oxide content of the coatings is high due to the oxidation of the molten material by the effect of atomizing air and the entrainment of the surrounding air into the spray stream. This increase in oxide content will increase the hardness of the coatings, improving the abrasion and wear resistance. However, the oxide content is detrimental to the coating, since oxides will reduce the adhesion strength between the coating and the substrate and will cause problems during machining. Additionally, using atomizing air will produce coatings with relatively high porosity, which is detrimental. Although, increasing the flow of the atomizing air will lead to higher adhesion of the coating to the substrate due to the increase of the viscous force and surface tension force. Another disadvantage of atomizing air is the burn-off of alloying elements contained in wires. These elements are essential to produce the required characteristics of the coatings [29], [38], [39]. As a consequence, the coatings cannot be produced reliably. However these disadvantages can be overcome using nitrogen as atomizing gas. Nitrogen

will produce coatings with lower oxide content and porosity. The use of nitrogen in arc spray can stabilize the fluctuation of arc length and voltage even at lower current [25], [44].

The adhesion of the coatings depends on the interactions between individual lamellae and between lamellae structure and substrate. The bond strength of the coatings is affected by the physical and chemical interactions between the coating and the substrate and by the microstructure of the interfacial area. Poor adhesion can be related to poor interfacial interlocking, low degree of metallurgical bonding and high internal stresses. The degradation modes of the coatings depends on the nature of the interface between the coating and the substrate and on the chemical phenomena that occur at the interface through deposition and solidification [29].

As mentioned before, sprayed coatings are the result of the impact, deformation and rapid solidification of individual molten droplets so, due to that, the structure of the coatings consists of a succession of overlapping lamellae. It is known that faster molten particles have smaller size and higher kinetic energy, and, owing to this, these particles will spread and deform more readily on impact, which will lead to coatings with higher density and lower amount of porosity. That results in better wettability, yielding greater accommodation of the particles and thus coatings more homogeneous. However, as aforementioned, small particles have relatively big surface area which means that during the flight, they will oxidize on bigger degree comparing with bigger size droplets, increasing the possibility of oxide inclusions. On the other hand, as the small particles have higher velocity, they will have shorter fly duration and less time for the occurrence of oxidation reactions. The coating structure at the instant of impact on the substrate is determined by the particle temperature and velocity. At the moment of impact, the molten particles will spread out radially in the form of thin disks. In reality, however, the deposit is not uniform in thickness, and the periphery of the flattened particle is not circular [29], [38].

In arc spray, at lower power and current, the particles get cooled and their velocities are reduced. This will lead to a larger number of unmelted particles which results in high porosity and micro cracks [43].

1.2.2. Comparison between flame and arc spray

Flame and arc spray have several differences between them and there are many studies in the literature that compare these techniques.

From a wider viewpoint, there are several books in the literature that compare all the thermal spray processes. Table 1.3 shows a wider comparison between flame and arc spray.

Table 1.3 - Wider comparison between flame and arc spray [30].

Parameter/Property	Flame spray	Arc spray
Gas flow (m ³ /h)	71	71
Flame/arc temperature (°C)	2800	5500
Particle velocity (m/s)	180	240
Relative adhesive strength (a) ¹	4	6
Cohesive strength	Medium	High
Oxide content (%)	4	0.5 - 3
Relative process cost (a) ¹	3	1
Maximum spray rate (kg/h)	9	16

¹ (a) 1 (low) to 10 (high)

Flame spray is more expensive than arc spray, and produces coatings with lower adhesive and cohesive strength with higher oxide content. In terms of costs for zinc spraying, Malek et. al [19] studied the differences between these techniques (Table 1.4).

Table 1.4 - Comparison of costs between flame and arc spray [19].

Characteristic	Flame spraying	Arc spraying
Liquefaction of zinc (kg/h)	18	35
Energy costs for zinc (\$/h)	28	25
Effective use (min/h)	40	40
Effective use (kg/h)	12	23
Energy costs (\$/m ²)	2.33	0.11
Spraying speed (m ² /h)	12	23
Wage costs (\$/m ² at 60\$/h)	4.17	2.17
Total costs (\$/m ²)	6.50	2.28

In terms of costs, flame spray have the highest production cost, as shown in table 1.4. Arc spray is more cost effective due to its high efficiency and deposition rate [43].

1.3. Temperature humidity bias test

The expected lifetime of the electronic products is continuously increasing. Due to that, each electronic component must ensure the same expected lifetime. Metallized film capacitors are quite cheap and can be produced easily, however due to their popularity, there is a continuous pressure due to the market demands for size reduction and cost savings. This means that the producers apply cheaper foils and alloys to produce thinner dielectrics and metal foils and thus, reducing the costs. This reduction combined with the environmental conditions such as high temperatures and humidity levels under applied voltage, decreasing the performance of the metallized film capacitors. Such policy results in restrict demands on controlling their production process. Especially for passive components, the degradation modes are quite unknown [6], [17], [45].

Actually, metallized film capacitors should be optimized to provide the customer a well-defined level of reliability through the expected lifetime. Metallized film capacitors are quite sensitive to temperature and humidity. Due to that, in order to evaluate the capacitors sensibility to the environmental conditions, an accelerated lifetime test, such as temperature humidity bias test, is necessary. Moreover, testing of the film capacitors can save time and cost in processing. On the other hand, it is important to perform temperature humidity bias test that is a relatively short term test to identify the long term behavior. Originally, this test was designed to accelerate moisture penetration into non-hermetic integrated circuit packages in order to originate corrosion failures in the metallization. In a temperature humidity bias test, the component is put at elevated temperatures and humidity under bias for a long period of time. The most common test is biased 85°C/85% RH test. In this test, the components are exposed at 85°C and 85% relative humidity during 1000 hours. When evaluating the test results, it should be differentiated if the results are caused by an aging process (predictable) or by a degradation process (destructive) [5], [6], [26], [46], [47].

Vishay wants to include this test as a part of the component qualification process to ensure that the film capacitors have enough robustness for the application.

CHAPTER 2 - Experimental Methodologies

2.1. Film metallizations

Vishay uses several types of film metallizations for their capacitors, with different materials of dielectric and metallic plate, with a broad range of thicknesses, and from different suppliers. In film metallizations, the metal layer usually is aluminum, zinc or an aluminum-zinc alloy (Figure 2.1).



Figure 2.1 – Film metallizations (Vishay).

In the first stage of this work, four types of film metallizations were analyzed (Table 2.1):

Table 2.1 – Designation with the reference, the supplier and the dimensions of the four types of film metallizations.

Designation	Reference	Supplier	Thickness (μm)	Width (mm)
F1	80855523	A	3	50
F2	80855896	A	5.8	26
F3	80900984	A	4.8	75
F4	80855775	A	3	26

In some electrical tests it was found a difference between electrical properties of two film metallizations with the same thickness but of different suppliers. In this way, for the second stage, the difference between these two film metallizations was evaluated (Table 2.2):

Table 2.2 - Designation with the reference, the supplier and the dimensions of the two types of film metallizations.

Designation	Reference	Supplier	Thickness (μm)	Width (mm)
F5	80855719	A	4.8	50
F6	80855719	B	4.8	50

Vishay Electrónica Portugal produces several capacitor types, however, in this work, the film metallizations studied are those used for the 1848 capacitor type (Figure 2.2).



Figure 2.2 – 1848 film capacitor [48].

2.1.1. Winding

Winding is the process where the film metallizations are alternately rolled up in order to form a cell. The cell has three parts: in the center, the cell is formed by a non-metallized film, which works as mechanical support; in the middle is the active part of the capacitor, which is formed by the film metallization; the outermost part is the label that is formed by polypropylene film to serve as cell protection (Figure 2.3) [49].

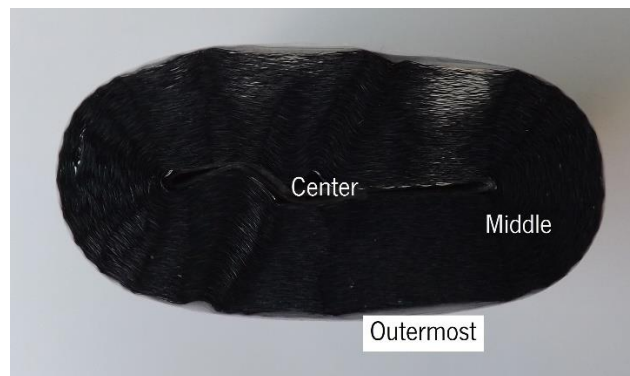


Figure 2.3 – Cell with the designation of the three parts (Vishay).

During this process, there are several factors that are required to take into account [49]:

- Film tension: this tension is maintained to avoid the shrinkage or the rupture of film and it is used a pressure roller to avoid air gaps between them;
- Pressure roller;
- Displacement: provides the isolation between the films during metal spray;
- Film length.

In this way, the parameters used in the winding of the film metallizations studied are presented in Table 2.3.

Table 2.3 – Parameters used in winding of the film metallizations.

Parameter	Value
Pressure roller diameter (mm)	12
Displacement (mm)	0.70 ± 0.20
Number of windings in the active part	988 ± 1
Length of the active part (cm)	6 784.07
Number of total windings	1 011.85

There are several machines in the winding division in Vishay Electrónica Portugal, however for 1848 capacitor type are used KOEM machines. After winding, the cell is pressed in order to remove the air gap in Lauffer machine.

2.1.2. Electrochemical corrosion tests

Corrosion will occur whenever are present an anode, cathode, return current path and electrolyte. Electrons will flow through the electrolyte at different current potential and will causing corrosion. Differences in potential can be caused by galvanic action, differential aeration in electrolyte or impurities in metal leading to pitting corrosion [19].

In capacitors, corrosion in film metallization is a problem. Once corrosion begins, the capacitor will began to loose capacitance, and in extreme cases, its viability. In this way, necessary tests are required to evaluate the corrosion behavior of the film metallizations. Electrochemical corrosion tests are a good approach to evaluate the corrosion rates and behaviors with the variation of chemical composition [50], [51].

These tests were conducted in distilled water at room temperature. The measurements employ a potentiostatic circuit which includes a three-electrode electrochemical cell (Figure 2.4), where saturated calomel electrode (SCE) was used as the reference electrode (all the potentials are given with reference to this electrode), Pt electrode was used as the counter electrode and the film metallizations were used as working electrodes.

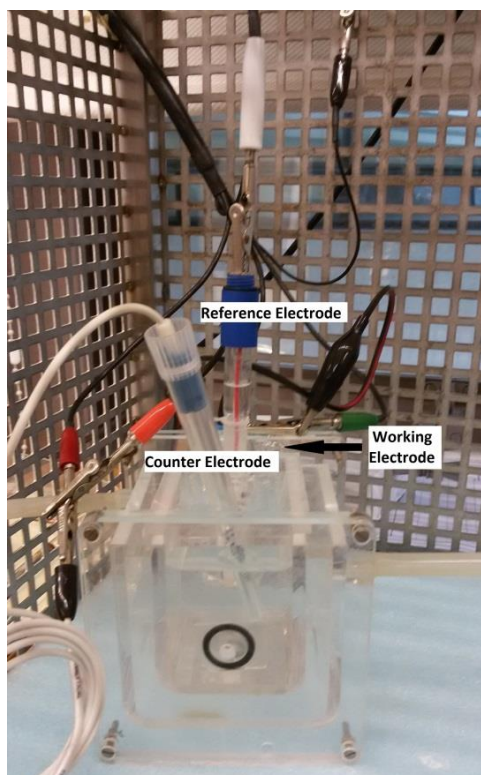


Figure 2.4 – Three-electrode experimental electrochemical cell (Dept. Physics, Univ. Minho).

First, the open circuit potential (OCP) was measured during one hour in order to stabilize the surface followed by potentiodynamic polarization (PD) from -1V to 2V with a scan rate of 1mV/s. All tests were performed in a Gamry Potentiostat Reference 600.

2.1.3. Atomic force microscopy

In atomic force microscopy (AFM), the sample is scanned by a cantilever with a sharp probe in the end. When the probe approaches the sample surface, the forces between the probe and the sample will lead to a deflection of the cantilever according to Hooke's law. The forces that are implicit in AFM are mechanical contact force, van der Waals forces, capillary forces, chemical bonding, electrostatic forces and magnetic forces. The deflection of the cantilever is usually measured using a laser spot reflected from its top surface onto an array of photodiodes. A feedback mechanism makes it possible to adjust the distance between the probe and the sample in order to maintain a constant force between them. Therefore, the sample is moved in the z direction by a piezoelectric tube and in the x and y directions for scanning the sample. With AFM it is possible to obtain three-dimensional (3D) surface profile with high resolution. The maximum depth is in the order of 10 – 20 μm and a maximum scanning area of 150 \times 150 μm [52].

This characterization technique was performed in F5 and F6 film metallizations in order to study the surface topography and evaluate the differences between them. The test was performed

in a Multimode Digital Instruments with a NanoScope III controller (Figure 2.5) using NCHV probes from Bruker.



Figure 2.5 – Atomic force microscopy equipment (Labmat, University of Minho).

With this characterization technique it is possible to extract the average roughness (R_a) in nanometers and this value is the average deviation of all points in the roughness profile from a mean line over the evaluation length, and is given by:

$$R_a = \frac{1}{N} \sum_{j=1}^N |r_j|$$

Where N is the number of sample points evaluated and r_i the absolute value of the profile deviation from the mean line [53].

2.1.4. Energy Dispersive X-ray Spectroscopy (EDS)

In the scanning electron microscope (SEM), an electron microprobe analyzer is used to realize chemical analysis in selected areas of the samples. In this way, energy dispersive X-ray spectroscopy provides a quantitative chemical composition of the film metallizations [33]. This is an important technique since it can see if the metallization has impurities and its difference, in the chemical compositions. The equipment used was an EDAX – Pegasus X4M (Figure 2.6).



Figure 2.6 - Energy dispersive X-ray spectroscopy equipment (SEMAT-UM, Guimarães) [54].

2.2. Metallizations

Figure 2.7 presents a cell with the metallization that is applied and the terminals.

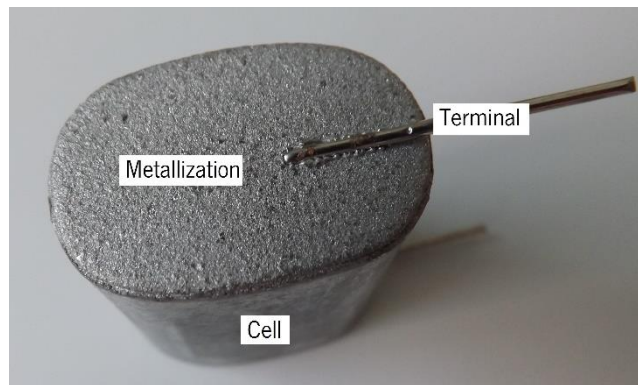


Figure 2.7 – Cell with the metallizations applied and the terminals.

Vishay uses five metal and alloy types to apply in the two metallizations layers. The following metallizations are applied in the first layer:

- Zinc (Zn);
- Zinc with 15% wt. aluminum (Zn-Al15);
- Aluminum (Al).

The chosen material depends on the capacitor type, and is applied to promote bonding between the cell and the solder (tin).

The base material of the second layer has to be tin alloy in order to enable soldering. Due to this, in the second layer the following metallizations can be applied:

- Tin with 3% wt. copper (Sn-Cu3);
- Tin with 30% wt. zinc (Sn-Zn30).

The materials properties used in the five metallizations types are presented in table 2.4.

Table 2.4 – Materials properties used in the five metallizations types [55]–[58].

	Material	Zn	Al	Sn	Cu
	Property				
	Density (g/cm ³)	7.10	2.70	7.29	8.96
Mechanical	Hardness (Vickers)	30	15	4	49
	Elasticity modulus (GPa)	96.5	68	44.3	117
Elect.	Electrical resistivity (Ω.cm)	5.92×10 ⁻⁵	2.70×10 ⁻⁶	1.15×10 ⁻⁵	1.72×10 ⁻¹⁰
Thermal	Coefficient of thermal expansion (CTE) (μm/m.°C)	31.2	25.5	23.8	16.4
	Thermal conductivity (W/m.K)	112.2	210	63.2	401
	Melting point (°C)	419.58	660.37	231.97	1084.62

In order to analyze the microstructure of the metallizations, the samples were metallographically prepared: first, they were grinded down to 2500 mesh size SiC paper and polished with diamond suspension (1 μm). After polishing, all samples were cleaned with distilled water and propanol and were examined in a Nikon Optiphot – 100 optical microscope (OM) equipped with a Leica EC3 digital camera.

2.2.1. Flame and arc spray

The metallization used on top of the thin film capacitor cell is applied by flame or arc spray, and the method depends on the capacitor type. These techniques have several parameters that require adjustment. In tables 2.5 and 2.6 are presented the parameters used in flame and arc spray of Vishay and the parameters found in the literature.

Table 2.5 – Comparison between the flame spray parameters used in Vishay and those mentioned in the literature [30], [33].

<u>Parameters</u>	<u>Vishay</u>	<u>Literature</u>
Gas types	O ₂ , propane	O ₂ , acetylene or propane
Oxygen to fuel ratio	-	1:1 or 1.1:1*
Spray distance (mm)	400 - 230	120 - 250
Diameter of the wires (mm)	3.175	3 – 6 (typically 2.3, 3.17 and 4.75)
Gas flow (l/min)	10.5 and 39	100-200
Flame velocities (m/s)	-	50-100
Flame temperatures (°C)	-	2727-3077

* Adjusting the fuel/oxygen ratio, either side of stoichiometry, will cool the flame. The reason behind this adjustment is to make the flame either oxidizing or reducing. Flames are set to be reducing (fuel-rich) in order to minimize oxidation.

Table 2.6 - Comparison between the arc spray parameters used in Vishay and those mentioned in the literature [30], [33], [38].

<u>Parameters</u>	<u>Vishay</u>	<u>Literature</u>
Gas types	Air	Air, Nitrogen
Arc voltage (V)	10	20 - 40
Arc current (A)	-	50 - 350
Spray distance (mm)	160 - 600	50 - 170
Diameter of the wires (mm)	2	1.6 – 5.0
Atomizing gas flow (l/min)	8.1 - 690	20 - 1300
Atomizing gas pressure (MPa)	-	0.2 – 0.7
Electric power (kW)	-	5 - 10

As can be seen, there are some differences in the parameters that Vishay uses compared with those in the literature. In this way, this is a necessary comparison since it may explain the differences between the microstructures of the metallizations with the microstructures in the literature.

2.2.2. Measurement of in-flight particles

It is well known that the particle size and shapes will affect the coatings properties. So in this way, the measurement of in-flight particles is a technique that supports this study and helps to understand the coating behavior.

The Al, Zn, Zn-Al15, Sn-Zn30 and Sn-Cu3 particles processed by flame spray for the same metallization thickness (225 μm) were captured before the impact in the substrate. For that, plastic cases were covered with a grid and with water inside, to obtain the particles (Figure 2.8).

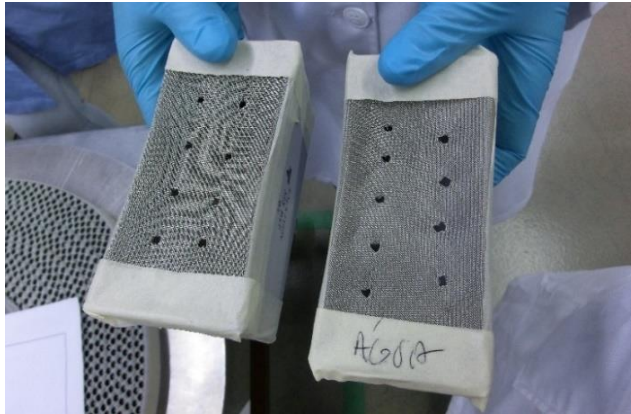


Figure 2.8 – Plastic cases with grid to obtain the particles before the impact.

After that, the plastic cases were placed in the substrate of the flame spraying machine (Figure 2.9).



Figure 2.9 – Plastic cases in the substrate of the spraying machine (Vishay).

After the spraying process in the plastic cases, the particles were obtained through the filtration of the water (Figure 2.10).

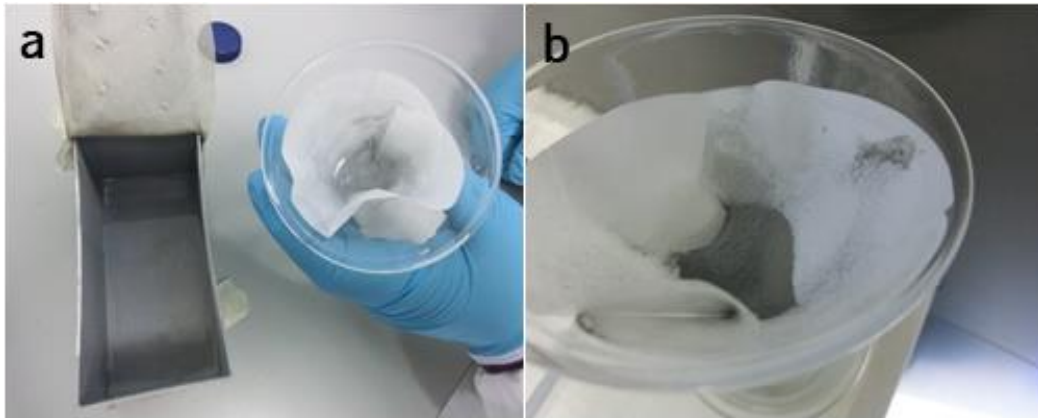


Figure 2.10 – a) and b) water filtration of the particles.

After the filtration process, the particles were observed in the Nikon Optiphot – 100 optical microscope (OM) equipped with a Leica EC3 digital camera with aim to calculate the particle size through Gwyddion software.

2.2.3. Standard test method for water vapor transmission of materials

This standard (E96-95) [59] enables the determination of water vapor transmission (WVT) of materials through which the passage of water vapor may be of importance. With this test it is possible to estimate the water vapor transmission, the permeance and the average permeability. Permeability is the arithmetic product of permeance and material thickness [59]. The result of this test is very interesting for this work since it is possible to test the permeability of each metallization (Zn, Al, Zn-Al15, Sn-Cu3 and Sn-Zn30) and thus determine the better metallization for protect the cell against humidity for biased 85°C/85% RH test.

In this way, four metallization types (Zn, Zn-Al15, Sn-Cu3 and Sn-Zn30) were tested with the same thickness (225 μm) and two Zn samples processed by ABM machine with different thicknesses. ABM machine is an arc spray machine with a different system. In addition, samples with two layers (Zn-Al15 – Sn-Cu3) with different thicknesses were also tested.

Table 2.7 shows the samples with the thicknesses and the method that were studied in terms of permeability.

Table 2.7 – Samples with the thicknesses and the method that were tested.

Material	Spray method	Thickness (μm)
Zn-Al15	Flame	225
Sn-Cu3	Flame	225
Zn	Flame	225
Sn-Zn30	Flame	225
Zn ABM*	Arc	225
Zn ABM*	Arc	800
Zn-Al15 – Sn-Cu3	Flame	225-145
Zn-Al15 – Sn-Cu3	Flame	225-225
Zn-Al15 – Sn-Cu3	Flame	275-325
Zn-Al15 – Sn-Cu3	Flame	325-325

*ABM machine is an arc spray machine with a different system compared with the others

According to the standard E96-95 [59] there are two methods: water and desiccant method. The method used was the desiccant method. In this method, silica gel was used as desiccant. The test dishes (glass water) were filled with desiccant to cover the bottom and after that, the samples were attached to the dish with silicon glue (Figure 2.11).

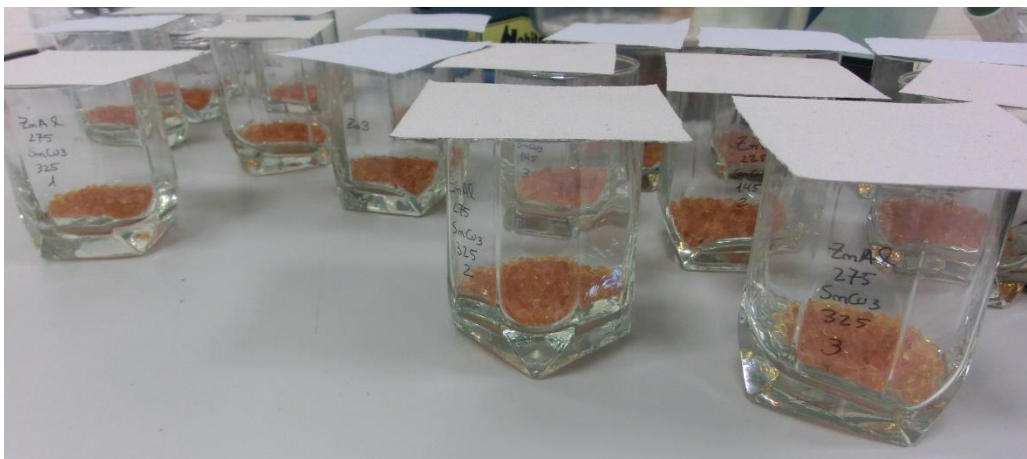


Figure 2.11 – Test dishes with the samples attached.

After test dish assembly, the dishes were weighed in a Sartorius AX 224 analytical balance (Figure 2.12a) before entering the climatic chamber (FITOCLIMA chamber – Aralab) at 85°C and 85% relative humidity (Figure 2.12b).



Figure 2.12 – a) Weight of the test dishes (Vishay); b) Climatic chamber (Vishay).

The test dishes were weighed periodically in order to provide enough data points during the test and enable the calculation of metallizations permeability.

2.2.4. Scratch test

Scratch test is usually used to characterize the coating adhesion to a substrate. In this test, a loaded diamond indenter is drawn across the coating surface under constant or an increase load. The acoustic emission (AE) is monitored during the scratching in order to determine more precisely the critical load (P_c) at which the failure takes place [52].

The aim of this test was to evaluate the adhesion of the several metallization types to the cell and it was performed in all the combination of the metallization layers used in Vishay with total thickness of 500 μm (Table 2.8):

Table 2.8 – Samples tested in scratch test with thickness of 500 μm .

Metallizations	
First layer	Second layer
Zn (electric arc)	Sn-Zn30
Zn-Al15	Sn-Cu3
Al	Sn-Cu3
Zn-Al15	Sn-Zn30
Zn	Sn-Cu3
Zn	Sn-Zn30

The equipment used was Scratch Tester Revetest (Figure 2.13) with a progressive load since 0.9 N to 20 N, with a loading rate of 20 N/min and a speed of 10 mm/min.

**Figure 2.13** – Scratch test equipment (SEMAT-UM Guimarães) [60].

The indenter type used was Rockwell diamond (200 μm diameter), and during the test, the normal and frictional force, the friction coefficient, the acoustic emission and the penetration depth was recorded.

2.2.5. Thermal conductivity

As aforementioned, the metallization has to be a suitable thermal barrier in order to protect the cell against temperature. In this way, it is necessary evaluate the thermal conductivity of the metallizations to ascertain the better metallization to protect the cell against heat. This property

depends on the coating structure, defects, porosity, real contacts between splats and oxide content which are linked to the fabrication process [52].

The thermal conductivity was measured in the following samples:

- Sn-Zn30 – 225 μm ;
- Sn-Cu3 – 225 μm ;
- Zn – 225 μm ;
- Zn-Al15 – 225 μm ;
- Zn ABM – 225 μm ;
- Zn ABM – 800 μm .

In order to measure the thermal conductivity of the samples, first it was necessary measure the electrical conductivity. The electrical conductivity was measured in HMS-5300 Hall Effect Measurement System at different temperatures (27 - 77 °C) (Figure 2.14). The magnetic field applied was 0.56 T with a current of 20 mA.



Figure 2.14 - HMS-5300 Hall Effect Measurement System (Dept. Physics, Univ. Minho).

A test assembly was set with several components, as shown is Figure 2.15, in order to determine the thermal conductivity.

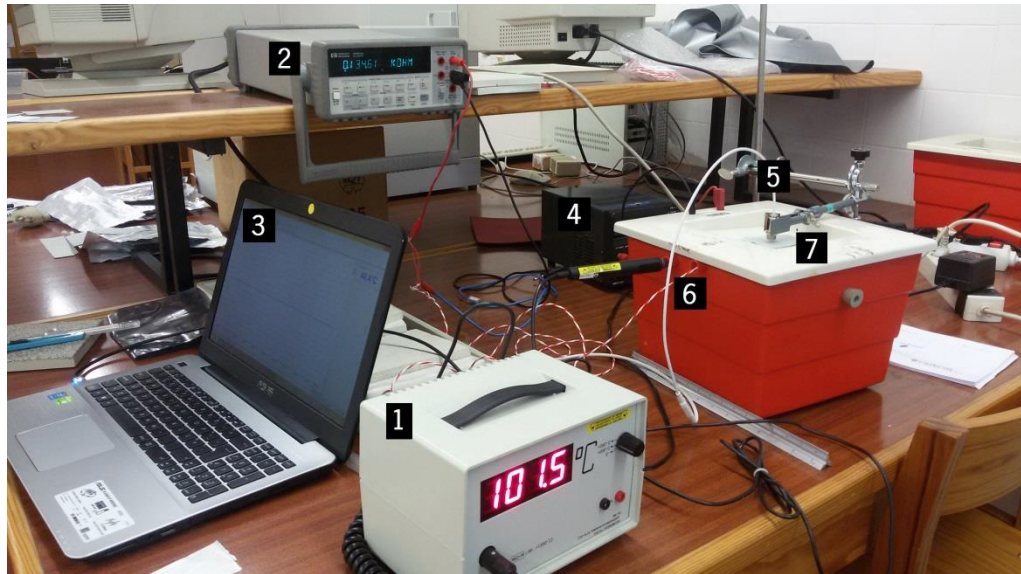


Figure 2.15 – Test assembly for thermal conductivity measurements: 1) Digital thermometer; 2) Multimeter; 3) Software; 4) Power supply; 5) Micro size infrared optical pyrometer; 6) Pt100 sensor; 7) Sample (Dept. Physics, Univ. Minho).

In this assembly it was used a digital thermometer LD 666 190, a multimeter (34401A) from Hewlett Packard, a DC power supply PS 613, a platinum thin-film temperature sensor (Pt100 sensor) from Innovative Sensor Technology and Optris® CSmicro LT infrared optical pyrometer and its software.

Through this test assembly, the temperatures in the Pt100 sensor and optical pyrometer were recorded for two temperatures (85°C and the maximum temperature that each sample reaches) in order to obtain the thermal conductivity from the following equation:

$$k = L_z \times \sigma \times T_{intern}$$

Where the k (in W/m.K) is the thermal conductivity, L_z (in W.Ω/K²) is the Lorenz factor, σ (in 1/Ω.m) is the electrical conductivity and T_{intern} (in K) is the temperature of the Pt100 sensor.

CHAPTER 3 - Results and discussion

3.1. Film metallizations

3.1.1. Electrochemical corrosion tests

In Figure 3.1 the evolution of open circuit potential (OCP) with time for F1, F2, F3 and F4 film metallizations (Table 2.1) is presented.

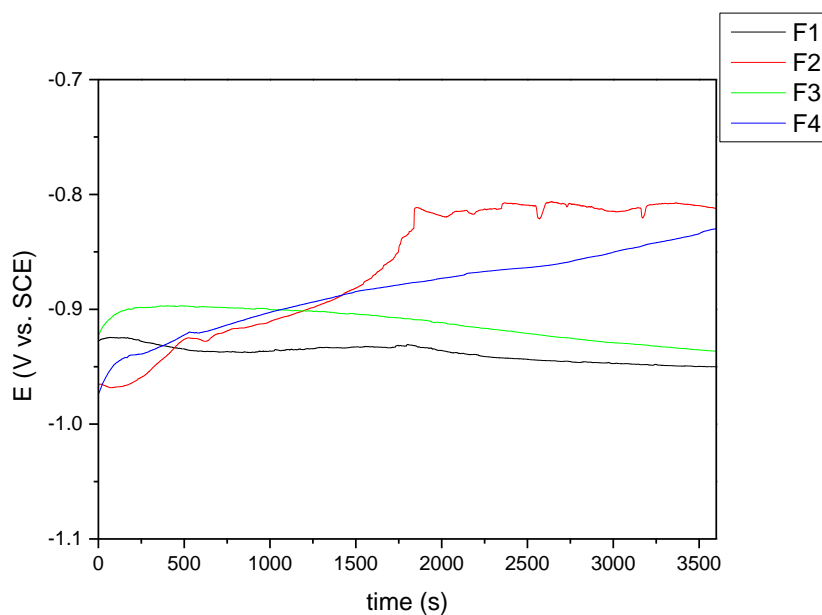


Figure 3.1 - Open circuit potential evolution with time for F1, F2, F3 and F4 film metallizations.

From OCP evolution, it is possible to see that the film metallizations have different behaviors. F2 and F4 film metallizations are in a passivate state since the OCP value increase with time and evolve for similar and higher values. On the other hand, F1 and F3 film metallizations are in a stable state since the OCP value does not change significantly with time and these two film metallizations evolve for similar and lower values of open circuit potential.

Figure 3.2 presents the potentiodynamic polarization curves (PD) for F1, F2, F3 and F4 film metallizations. In all the samples, the curves show three regions. The first region corresponds to cathodic domain, which includes all the potentials bellow corrosion potential (E_{corr}), in which the current density is given by the reduction of water and dissolved oxygen. The second region corresponds to active region where corrosion potential lies between E_{corr} and around -0.5V. The third region corresponds to the passive domain and is above -0.5V. In this domain, there is a passive

film formation. From these curves is possible to extract by Tafel extrapolation parameters such as corrosion potential (E_{corr}) and corrosion current density (i_{corr}) (Table 3.1).

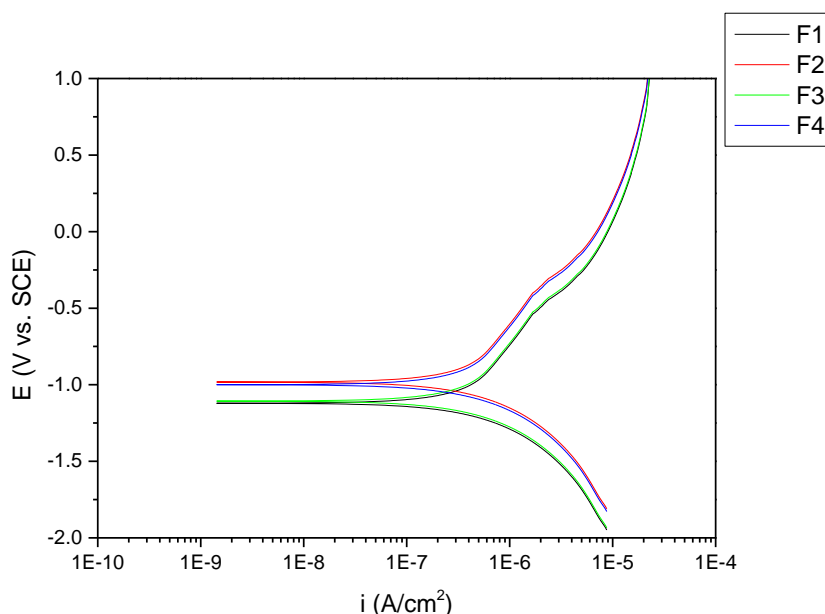


Figure 3.2 - Potentiodynamic polarization curves for F1, F2, F3 and F4 film metallizations.

Table 3.1 - E_{corr} and i_{corr} for F1, F2, F3 and F4 film metallizations.

	E_{corr} (V)	i_{corr} (A/cm ²)
F1	-1.09 ± 0.046	$7.21 \times 10^{-7} \pm 6.42 \times 10^{-8}$
F2	-0.85 ± 0.043	$1.03 \times 10^{-6} \pm 4.22 \times 10^{-7}$
F3	-1.02 ± 0.025	$4.29 \times 10^{-7} \pm 1.01 \times 10^{-7}$
F4	-0.85 ± 0.050	$2.27 \times 10^{-6} \pm 4.14 \times 10^{-7}$

As for the open circuit potential evolution, in the potentiodynamic polarization curves, the behavior of F2 is similar to F4 and F1 is similar to F3. F2 and F4 have higher corrosion potentials compared with the others, which means that these film metallizations have higher corrosion resistance. However, F2 and F4 film metallizations have higher corrosion current density values, which mean that these metallizations have higher corrosion rate. F1 and F3 have lower corrosion potentials, and thus lower corrosion resistance, however, due to their lower current density value, these film metallizations have lower corrosion rate.

Figure 3.3 and table 3.2 presents the Energy Dispersive Spectroscopy (EDS) results of F1, F2, F3 and F4 film metallizations and this test was performed in order to evaluate the local chemical composition of these film metallizations.

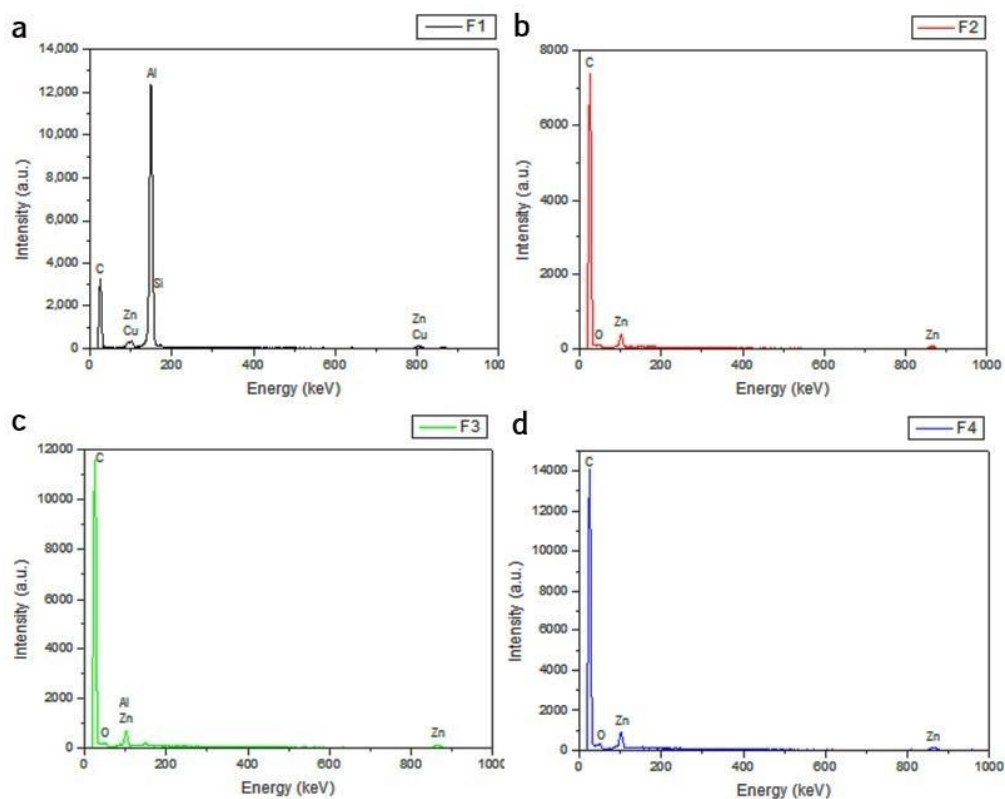


Figure 3.3 – EDS results for a) F1, b) F2, c) F3 and d) F4 film metallizations.

Table 3.2 – Quantification by EDS for the four film metallizations.

		Film metallizations			
		F1	F2	F3	F4
Elements (Wt %)	C K	59.51	90.89	89.36	88.38
	O K	-	4.84	5.67	6.71
	Al K	36.15	-	0.49	-
	Si K	0.49	-	-	-
	Cu K	2.49	-	-	-
	Zn K	1.36	4.28	4.47	4.91

As explained before, differences in potential are caused by galvanic action or impurities leading to pitting corrosion, and since F1 and F3 have other elements in their composition, this explains the lower corrosion potentials. On the other hand, F2 and F4 only have zinc in their compositions and thus, higher corrosion potentials. However, F1 and F3 have lower corrosion rates and this is probably due to the presence of aluminum in their compositions. The aluminum in the galvanic series is nobler than zinc, improving its corrosion behavior. The presence of carbon and oxygen is due to the polymer of the film metallizations.

Figure 3.4 presents the evolution of open circuit potential with time for F5 and F6 film metallizations.

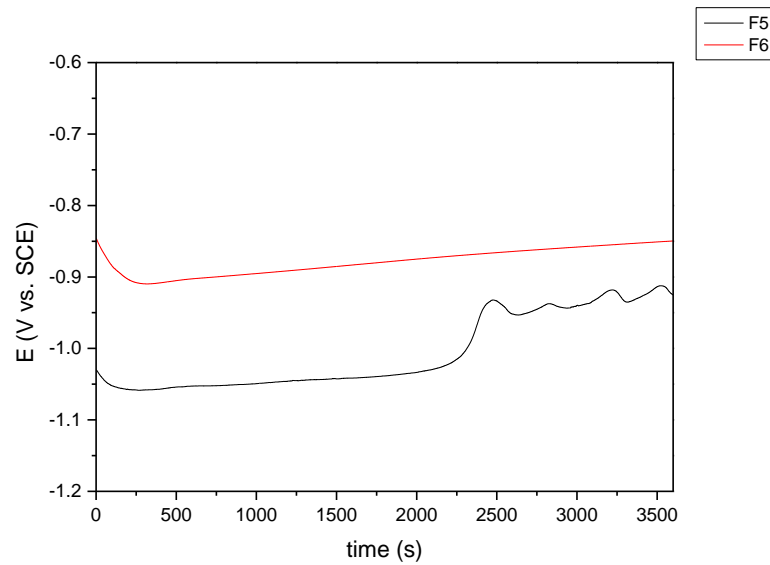


Figure 3.4 – Open circuit potential evolution with time for F5 and F6 film metallizations.

For both film metallizations, the variation from the initial value to the final value is not significant, which means that the samples are in a stable state.

Figure 3.5 presents the potentiodynamic polarization curves for F5 and F6 film metallizations. As in Figure 3.2 both curves show three regions: cathodic domain below corrosion potential (E_{corr}), active region where corrosion potential lies between E_{corr} and 0V for F6 film metallization and between E_{corr} and -0.25V for F5 film metallization and passive domain and is above 0V for F6 film metallization and -0.25V for F5 film metallization. The corrosion potential (E_{corr}) and corrosion current density (i_{corr}) are presented in Table 3.3.

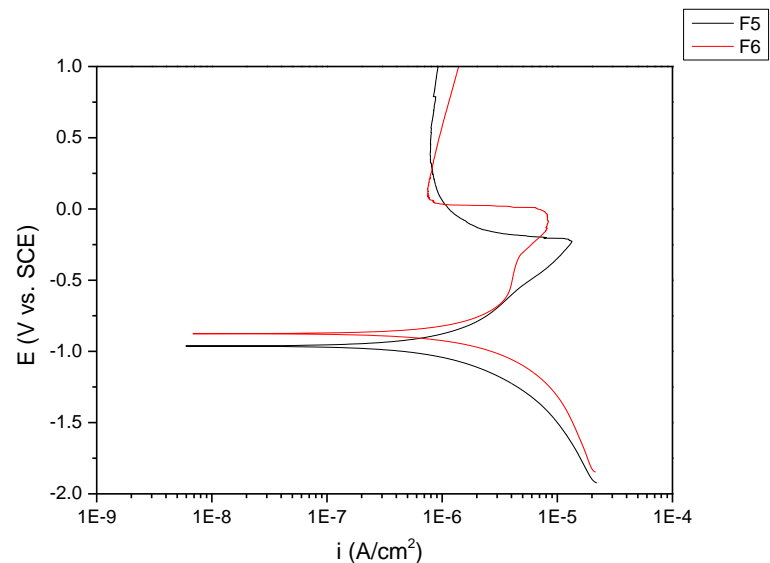


Figure 3.5 – Potentiodynamic polarization curves for F5 and F6 film metallizations.

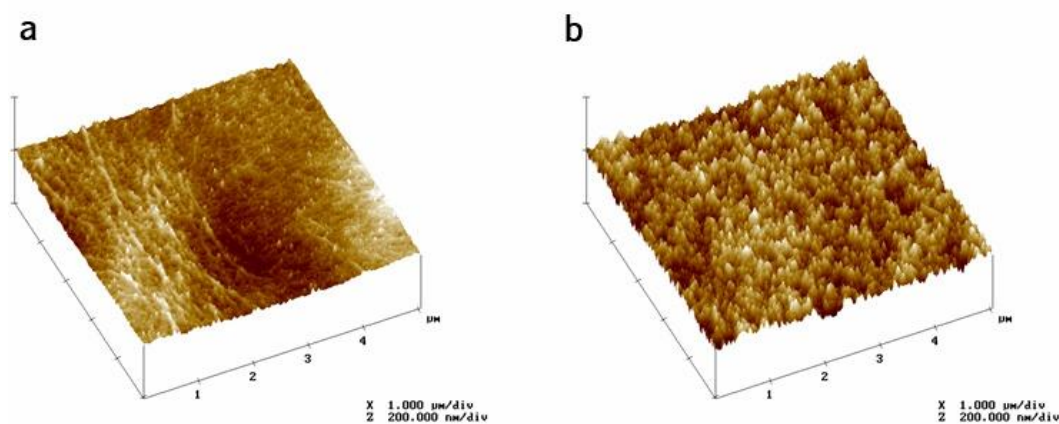
Table 3.3 – E_{corr} and i_{corr} for F5 and F6 film metallizations.

	E_{corr} (V)	i_{corr} (A/cm ²)
F5	-0.95 ± 0.023	$1.66 \times 10^{-6} \pm 7.22 \times 10^{-7}$
F6	-0.88 ± 0.001	$9.84 \times 10^{-6} \pm 1.74 \times 10^{-6}$

F6 film metallization have the highest E_{corr} value, which means that it has the highest corrosion resistance. The i_{corr} value represents the corrosion rate by a linear relation. The corrosion current density is higher for the F6 film metallization, which means that this film metallization has a higher corrosion rate than the F5 film metallization. Although the F5 film metallization has the lowest E_{corr} value (lowest corrosion resistance), this film metallization corrode slower than F6 film metallization.

3.1.2. Atomic force microscopy

The electrochemical corrosion results not explain the differences in the electrical test between F5 and F6 film metallization. Therefore, atomic force microscopy (AFM) was performed in order to understand this difference. In figures 3.6 and 3.7 it is possible to see the 3-D and 2-D superficial topography of F5 and F6 film metallizations.

**Figure 3.6** – 3-D view of superficial topography of a) F5 film metallization and b) F6 film metallization.

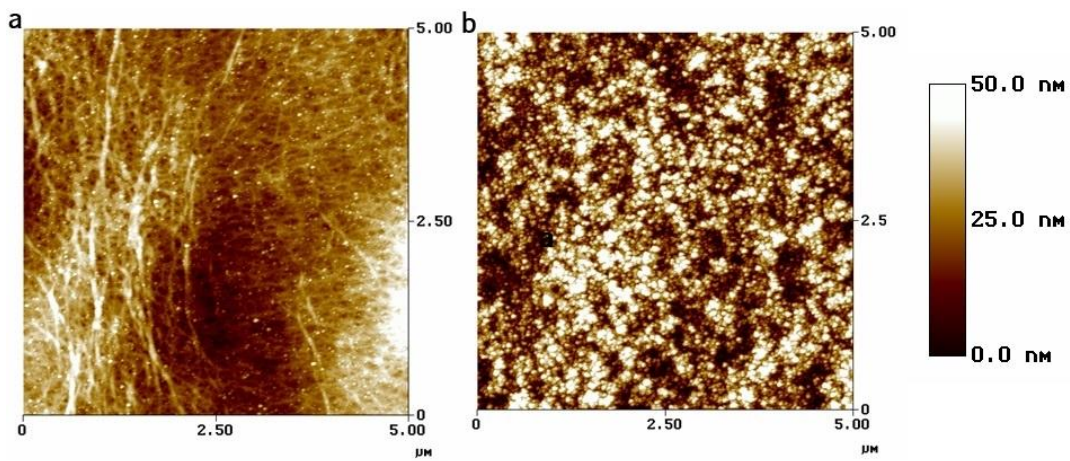


Figure 3.7 - 2-D view of superficial topography of a) F5 film metallization and b) F6 film metallization.

As mentioned before, through atomic force microscopy it is possible to extract the values of average roughness (R_a). In table 3.4 are presented the values for average roughness for both film metallizations (F5 and F6).

Table 3.4 – Roughness average (R_a) for F5 and F6 film metallizations.

	F5	F6
R_a (nm)	5 ± 1	10 ± 1

Figure 3.8 presents a boxplot with average roughness values for F5 and F6 film metallization, where it is represented the median and quadrilles (Q1 and Q3) values.

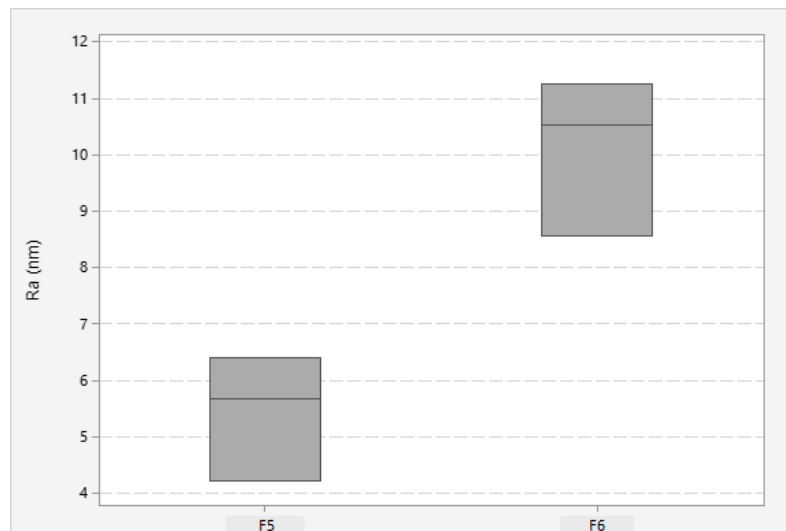


Figure 3.8 – Average roughness comparison between F5 and F6 film metallizations.

Based on these results, it is possible to conclude that F6 film metallization has a higher roughness value compared with F5 film metallization. After winding the film metallization in order to form a cell, this cell will be pressed, as aforementioned. Pressing a cell with film metallization

with higher roughness, will lead to poor electrical contact between the layers of film metallizations, and hence, reducing the electrical behavior. This is probably the cause of the differences in electrical performance, since as F6 film metallization has a higher roughness value, this will lead to poor compaction at pressing stage and, hence, will reduce the electrical contact between the films.

3.2. Metallizations

3.2.1. Measurement of in-flight particles

The measurement of in-flight particles was made in all the materials for metallizations for the same thicknesses (225 μm). In Figure 3.9 are presented the optical micrographs for Sn-Cu3, Sn-Zn30, Zn, Zn-Al15 and Al.

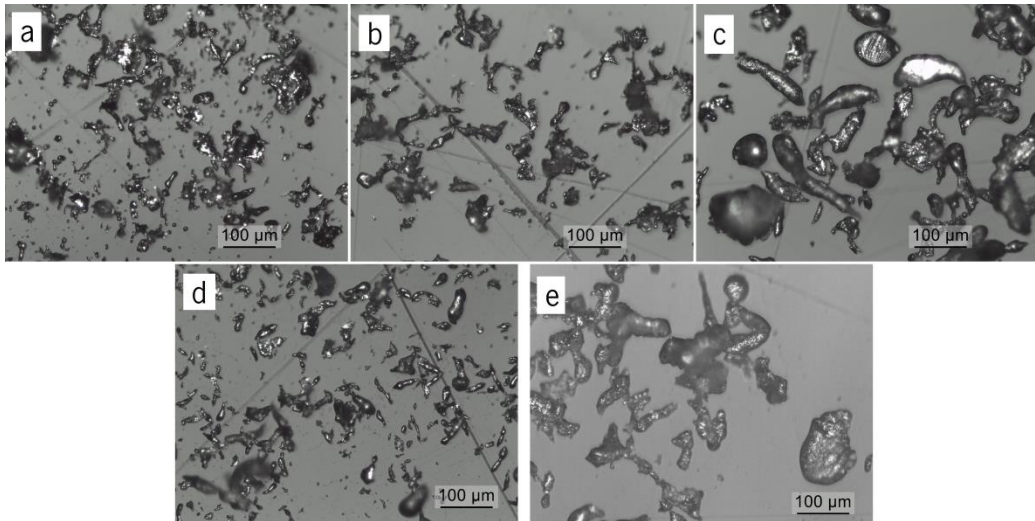


Figure 3.9 – Optical micrographs of particles for a) Sn-Cu3; b) Sn-Zn30; c) Zn; d) Zn-Al15 and e) Al.

Based on these images, it is possible to see that the grains shapes of all metallizations are irregular and different in size. Through Gwyddion software, it was possible to determine the particle size of each metallization. The values of particle size average are presented in table 3.5.

Table 3.5 – Values of particle size average for Sn-Cu3, Sn-Zn30, Zn, Zn-Al15 and Al.

	Sn-Cu3	Sn-Zn30	Zn	Zn-Al15	Al
Particle size (μm)	36 ± 14	39 ± 15	55 ± 17	33 ± 11	47 ± 16

In Figure 3.10 the boxplot with the particle size values for Sn-Cu3, Sn-Zn30, Zn, Zn-Al15 and Al is presented.

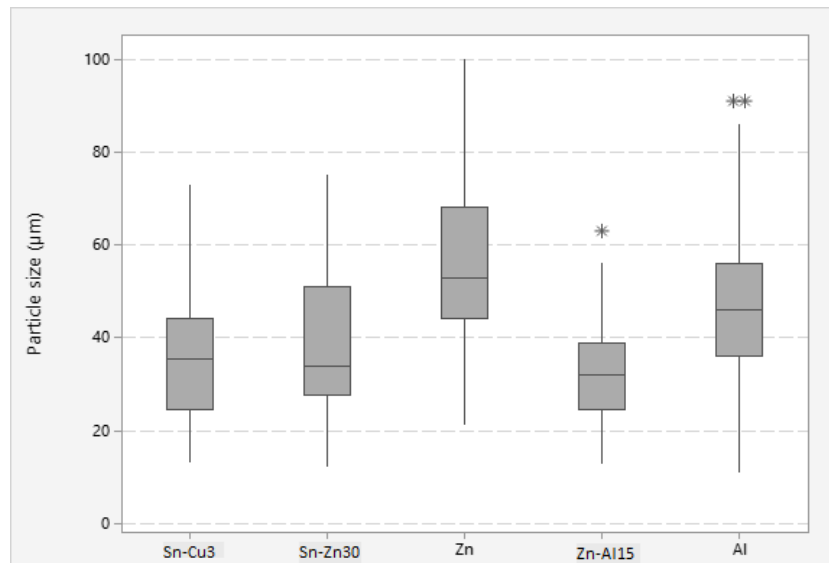


Figure 3.10 – Values of particle size average for Sn-Cu3, Sn-Zn30, Zn, Zn-Al15 and Al.

The pure materials (Zn and Al) have the biggest particle sizes when compared with the alloys (Sn-Cu3, Sn-Zn30 and Zn-Al15). In the literature it was found that these irregular shapes are detrimental for coating properties. For example, based on Johnston et al. [40], this irregular shape with long and cylindrical particles is the result of incomplete atomization. To avoid this and to produce particles with round and smooth surfaces, increasing atomizing gas pressure will increase the atomization and reduce the particle size, which will improve the coating properties.

3.2.2. Porosity

Porosity was measured with Gwyddion software aid. In table 3.6 are presented the porosity values for all tested samples.

Table 3.6 – Porosity values for all tested samples.

Sample	Porosity (%)
Al – Sn-Cu3	4.53 ± 1.87
Zn – Sn-Cu3	2.90 ± 0.47
Zn (electric arc) – Sn-Zn30	7.45 ± 2.48
Zn – Sn-Zn30	4.48 ± 1.37
Zn-Al15 – Sn-Cu3	1.75 ± 0.68
Zn-Al15 – Sn-Zn30	6.67 ± 2.84
Zn ABM (225 µm)	7.80 ± 1.48
Zn ABM (800 µm)	14.89 ± 2.40
Zn-Al15 (225µm) – Sn-Cu3 (225µm)	3.18 ± 1.03
Zn-Al15 (325µm) – Sn-Cu3 (325µm)	5.12 ± 1.28
Zn-Al15 (225µm) – Sn-Cu3 (145µm)	1.34 ± 0.46
Zn-Al15 (275µm) – Sn-Cu3 (325µm)	0.52 ± 0.23

The boxplot with the comparison of the porosity between the Al – Sn-Cu3, Zn – Sn-Cu3, Zn (electric arc) – Sn-Zn30, Zn – Sn-Zn30, Zn-Al15 – Sn-Cu3 and Zn-Al15 – Sn-Zn30 samples is presented in Figure 3.11.

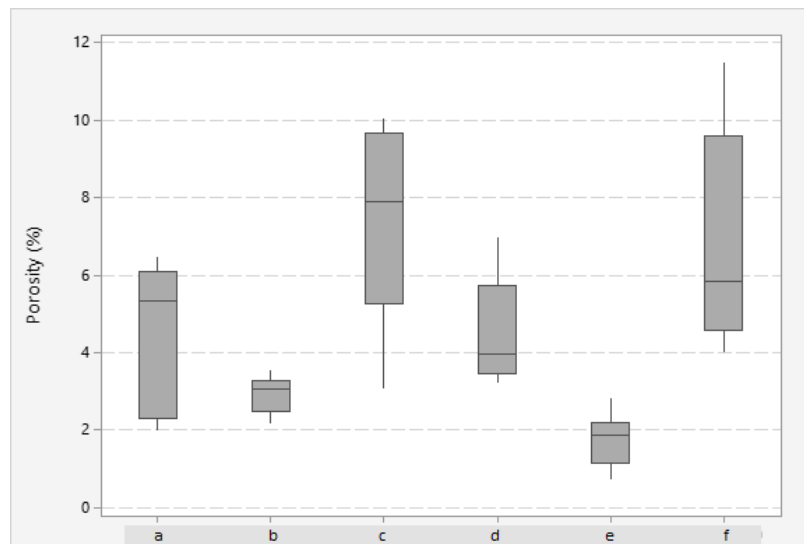


Figure 3.11 – Comparison of the porosity between: a) Al - SnCu3, b) Zn – Sn-Cu3, c) Zn (electric arc) – Sn-Zn30, d) Zn – Sn-Zn30, e) Zn-Al15 – Sn-Cu3 and f) Zn-Al15 – Sn-Zn30 samples.

Figure 3.12 shows the optical micrographs of the Al – Sn-Cu3, Zn – Sn-Cu3, Zn (electric arc) – Sn-Zn30, Zn – Sn-Zn30, Zn-Al15 – Sn-Cu3 and Zn-Al15 – Sn-Zn30.

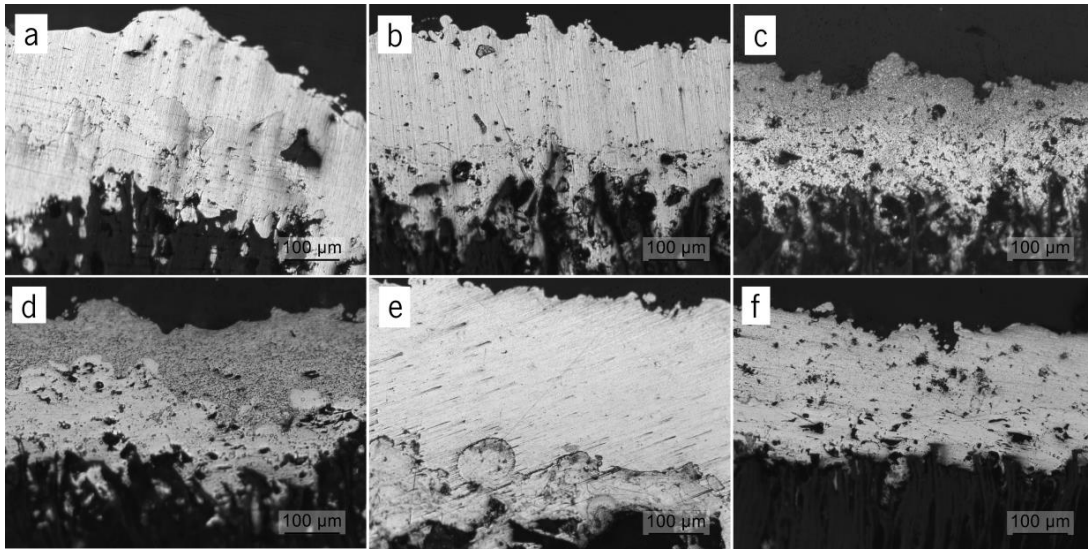


Figure 3.12 – Optical micrographs of a) Al – Sn-Cu3; b) Zn – Sn-Cu3; c) Zn (electric arc) – Sn-Zn30; d) Zn – Sn-Zn30; e) Zn-Al15 – Sn-Cu3 and f) Zn-Al15 – Sn-Zn30.

From the optical micrographs in Figure 3.12 is possible to observe some scratches due to the pull out of the oxides in the grinding. The sample with zinc processed by electric arc (Figure 3.12c) in the first layer is the sample that has the highest porosity value. This is probably due to the parameters of electric arc at Vishay are not optimized, producing samples with a high amount of defects such as porosity or oxides. The Al – Sn-Cu3 (Figure 3.12a), Zn – Sn-Zn30 (Figure 3.12d) and Zn-Al15 – Sn-Zn30 (Figure 3.12f) samples have approximately the same amount of porosity (around 5%). The Zn – Sn-Cu3 (Figure 3.12b) and Zn-Al15 – Sn-Cu3 (Figure 3.12e) are the samples with lower amount of porosity, where Zn-Al15 – Sn-Cu3 has the lowest value. As aforementioned, lower particle sizes leads to coatings with higher density and lower amount of porosity, and this is probably the reason why Zn-Al15 – Sn-Cu3 have the lower amount of porosity, since their particle sizes are smaller compared with the other materials.

The boxplot with the porosity comparison of the samples with different thicknesses produced by ABM machine is presented in Figure 3.13.

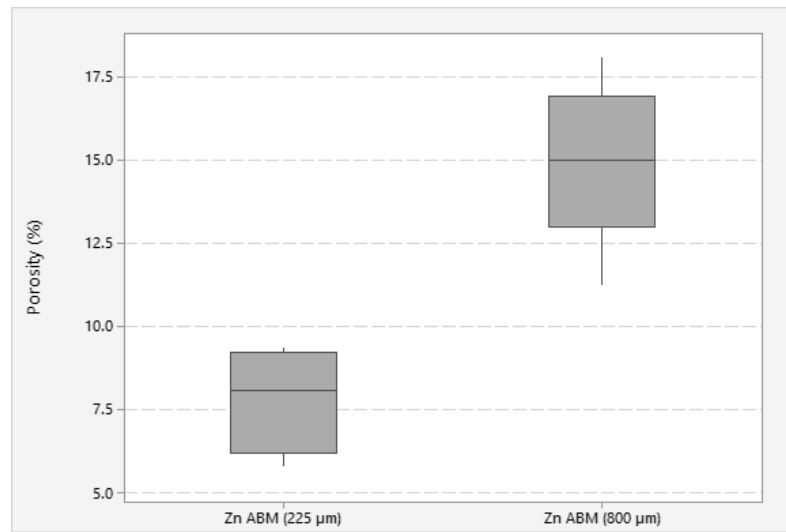


Figure 3.13 - Porosity comparison between the samples with different thicknesses produced by ABM machine.

Figure 3.14 shows the optical micrographs of the Zn ABM (225 μm) and Zn ABM (800 μm).

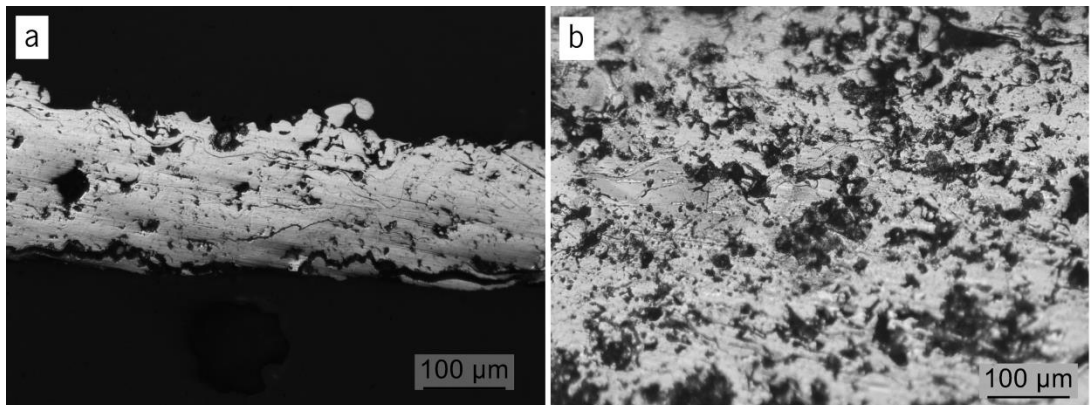


Figure 3.14 – Optical micrographs of a) Zn ABM (225 μm) and b) Zn ABM (800 μm).

With an increase in thickness, the probability of occurrence of defects is higher due to the higher amount of deposited material. In this way, as can be observed in Figure 3.14, the sample with 800 μm thickness (Figure 3.14b) has a higher porosity level than the sample with 225 μm thickness (Figure 3.14a).

The boxplot with the porosity comparison of the Zn-Al15 – Sn-Cu3 samples with different thicknesses is presented in Figure 3.15.

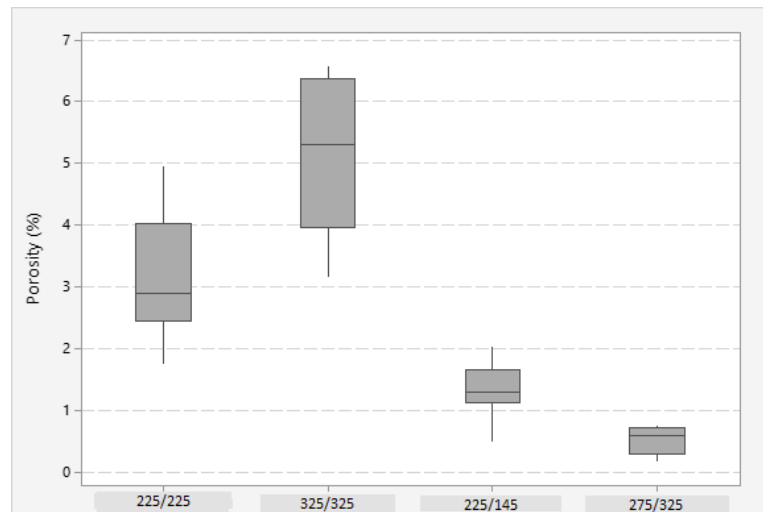


Figure 3.15 – Porosity comparison of the Zn-Al15 - SnCu3 samples with different thicknesses.

Figure 3.16 shows the optical micrographs of the Zn-Al15 (225 μm) – Sn-Cu3 (225 μm), Zn-Al15 (325 μm) – Sn-Cu3 (325 μm), Zn-Al15 (225 μm) – Sn-Cu3 (145 μm) and Zn-Al15 (275 μm) – Sn-Cu3 (325 μm).

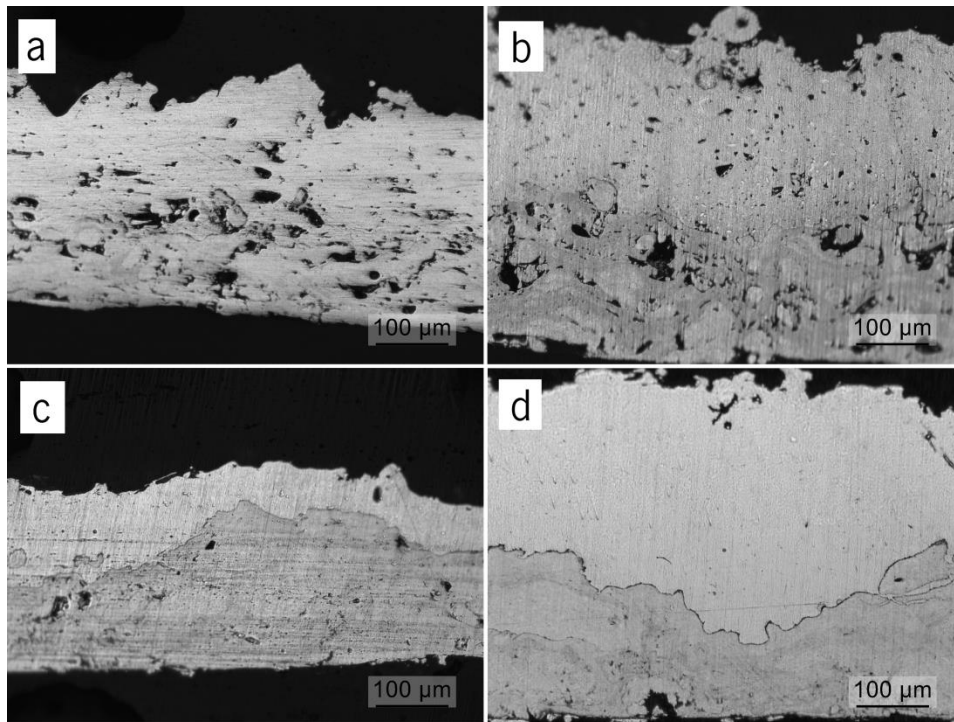


Figure 3.16 – Optical micrographs of a) Zn-Al15 (225 μm) – Sn-Cu3 (225 μm); b) Zn-Al15 (325 μm) - Sn-Cu3 (325 μm); c) Zn-Al15 (225 μm) – Sn-Cu3 (145 μm); d) Zn-Al15 (275 μm) – Sn-Cu3 (325 μm).

It was expected that the samples with higher thickness had higher porosity level due to high probability to occur defects such as porosity. This happens when comparing Zn-Al15 (225

μm) - SnCu3 (145 μm) to Zn-Al15 (225 μm) – Sn-Cu3 (225 μm) and Zn-Al15 (325 μm) – Sn-Cu3 (325 μm). However, the Zn-Al15 (275 μm) – Sn-Cu3 (325 μm) sample is the one with smaller porosity level, even when compared with Zn-Al15 (225 μm) – Sn-Cu3 (145 μm). This probably signifies that this condition is the optimum condition to process denser metallizations.

3.2.3. Permeability

The permeability average values for all tested samples are presented in table 3.7.

Table 3.7 – Permeability average values for all tested samples.

Sample	Permeability (perm)
Zn-Al15 (225 μm)	0.129 ± 0.006
Sn-Cu3 (225 μm)	0.006 ± 0.002
Zn (225 μm)	0.141 ± 0.004
Sn-Zn30 (225 μm)	0.007 ± 0.0004
Zn ABM (225 μm)	0.210 ± 0.003
Zn ABM (800 μm)	0.458 ± 0.007
Zn-Al15 (225 μm) – Sn-Cu3 (225 μm)	0.153 ± 0.044
Zn-Al15 (325 μm) – Sn-Cu3 (325 μm)	0.070 ± 0.065
Zn-Al15 (225 μm) – Sn-Cu3 (145 μm)	0.038 ± 0.010
Zn-Al15 (275 μm) – Sn-Cu3 (325 μm)	0.028 ± 0.022

The boxplot with permeability values for Zn-Al15, Sn-Cu3, Zn and Sn-Zn30 is presented in Figure 3.17.

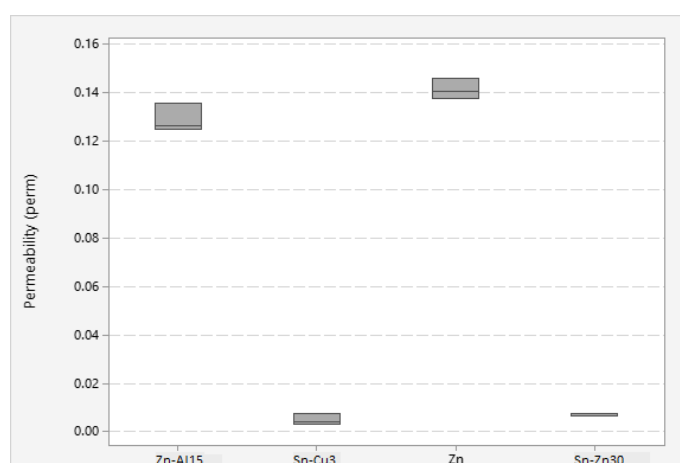


Figure 3.17 - Permeability values for Zn-Al15, Sn-Cu3, Zn and Sn-Zn30.

As it can be observed, there is a difference in the permeability values for Zn-Al15 and Zn when comparing to Sn-Cu3 and Sn-Zn30. The samples that contain tin (Sn-Zn30 and Sn-Cu3) have

the lowest permeability values. This can be explained due to the fact that tin acts as a sealant, in part, owing to its low melting temperature and due to the smaller particles sizes. As mentioned before, smaller particles will spread and deform more on the impact to the substrate, which leads to coatings with higher density, lower amount of porosity and thus, less permeable. Sn-Cu3 is the sample that has the lowest permeability, because only 3% wt. is copper and 97% wt. is tin, whereas in Sn-Zn30, 30% wt. is zinc and 70% wt. tin and due to the smallest particle size. On the other hand, Zn and Zn-Al15 are the samples more permeable, due to the bigger particle size which leads to coatings less homogeneous.

The boxplot with permeability values for Zn ABM (225 μm) and Zn ABM (800 μm) is presented in Figure 3.18.

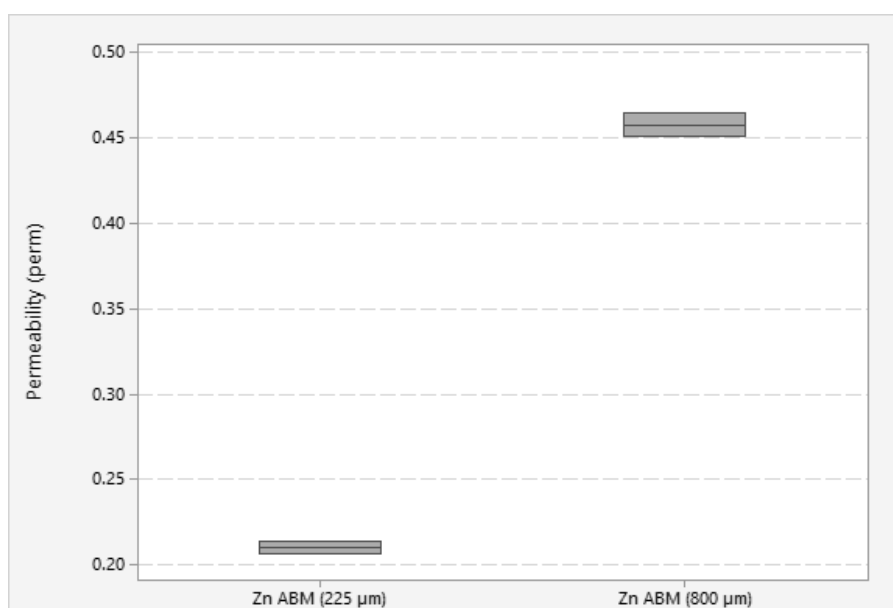


Figure 3.18 - Permeability values for Zn ABM (225 μm) and Zn ABM (800 μm).

As expected, the sample with 225 μm thickness has the lowest permeability value. This can be explained due to the amount of porosity. Zn ABM 800 μm has higher amount of porosity due to more material deposited which increases the probability to occur defects like pores. This leads to samples more permeable compared with Zn ABM 225 μm .

The boxplot with permeability values for Zn-Al15 (225 μm) – Sn-Cu3 (145 μm), Zn-Al15 (275 μm) – Sn-Cu3 (325 μm), Zn-Al15 (225 μm) – Sn-Cu3 (225 μm) and Zn-Al15 (325 μm) – Sn-Cu3 (325 μm) is presented in Figure 3.19.



Figure 3.19 - Permeability values for a) Zn-Al15 (225 μm) – Sn-Cu3 (145 μm), b) Zn-Al15 (275 μm) – Sn-Cu3 (325 μm), c) Zn-Al15 (225 μm) – Sn-Cu3 (225 μm) and d) Zn-Al15 (325 μm) – Sn-Cu3 (325 μm).

The Zn-Al15 (225 μm) – Sn-Cu3 (225 μm) and Zn-Al15 (325 μm) – Sn-Cu3 (325 μm) metallizations have the higher permeability values, which are in agreement with the porosity values. As it is well known, higher porosity level leads to more permeable metallizations. On the other hand, Zn-Al15 (275 μm) – Sn-Cu3 (325 μm) has the lowest porosity level, which justifies the lowest permeability value.

3.2.4. Scratch test

Scratch tests were made in thin film capacitor cells with metallizations of Zn – Sn-Cu3, Zn-Al15 – Sn-Cu3, Zn – Sn-Zn30, Zn-Al15 – Sn-Zn30, Al – Sn-Cu3 and Zn (electric arc) – Sn-Zn30. The cells were cut with thicknesses around 1 cm. In Figure 3.20 is presented an example of the tested samples (Zn-Al15 – Sn-Cu3) with and without the scratches.



Figure 3.20 - Tested samples (Zn-Al15 – Sn-Cu3) with and without the scratches.

As an example, the results given by the scratch test equipment for Zn-Al15 – Sn-Cu3 are presented in Figure 3.21.

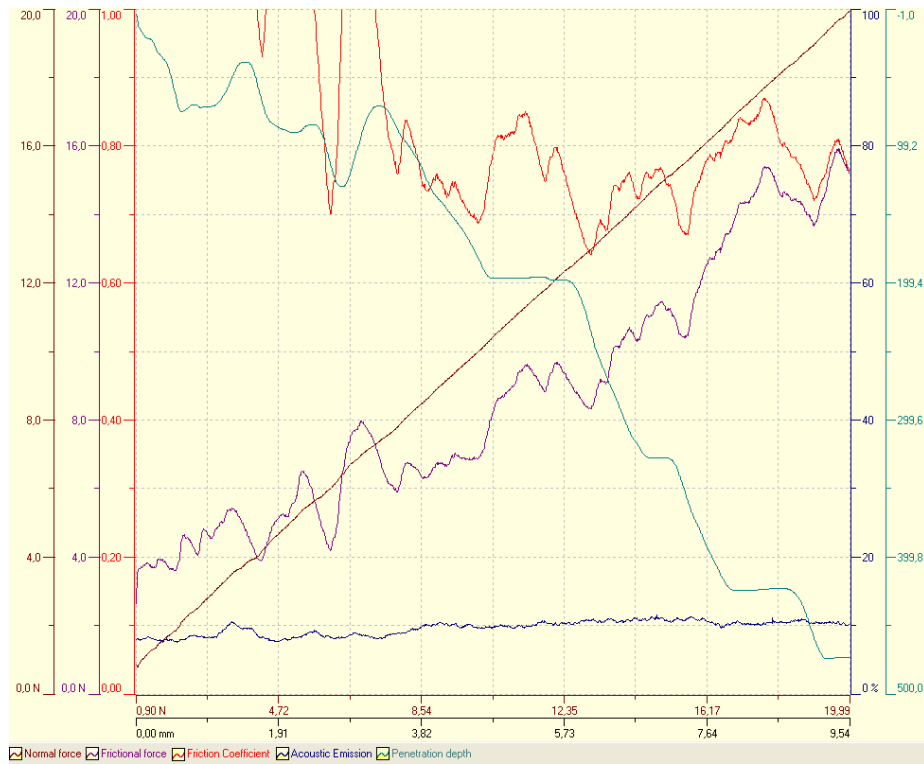


Figure 3.21 – Scratch test results for Zn-Al15 – Sn-Cu3.

For all tested samples the failure initiation was followed by optical microscopy observation. In Figure 3.22 is presented an example of the optical micrograph of the scratch for Zn-Al15 – Sn-Cu3 sample with the initiation of the cracks and the final spallation failure.

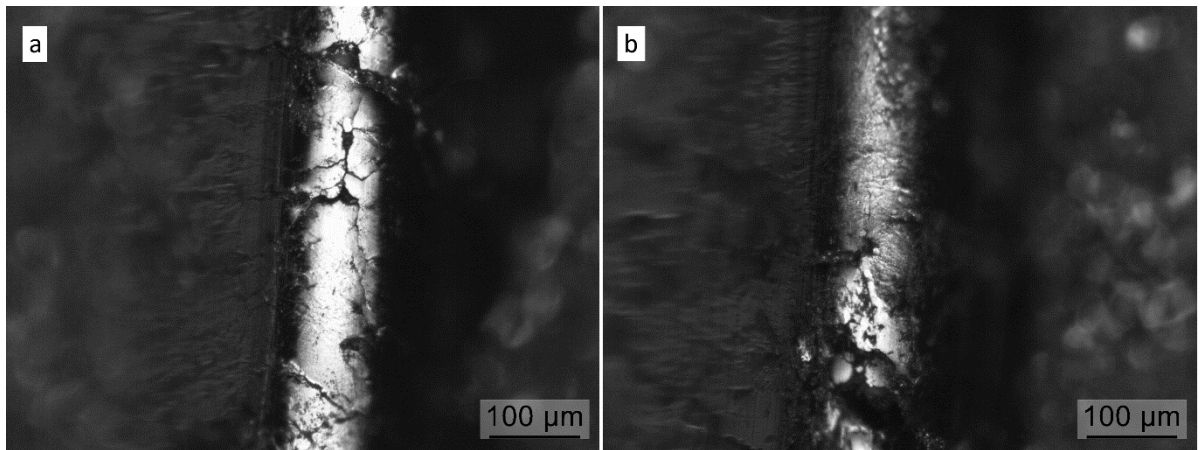


Figure 3.22 – Optical micrograph of the scratch for Zn-Al15 – Sn-Cu3 sample a) Initiation of the cracks; b) Final spallation failure.

The results of the failure initiation and critical adhesion failure load are presented in table 3.8.

Table 3.8 - Results of the failure initiation and critical adhesion failure load, relative to scratch length.

Sample	Failure (mm)	Critical adhesion failure load (N)
Zn – Sn-Cu3	6.7	15
Zn-Al15 – Sn-Cu3	6.2	19
Zn – Sn-Zn30	4.3	10.77
Zn-Al15 – Sn-Zn30	6.15	15.5
Al – Sn-Cu3	6.55	19
Zn (electric arc) – Sn-Zn30	4.85	13

These results can be related to the mechanical properties. The samples with lower adhesion to the substrate are those with lower mechanical adhesion. The metallizations that revealed lower adhesion to the capacitor cell were Zn – Sn-Zn30 and Zn (electric arc) – Sn-Zn30. As mentioned before, this poor adhesion can be related to low degree of metallurgical bonding and high internal stresses. This means that Zn – Sn-Zn30 and Zn (electric arc) – Sn-Zn30 samples are those with worst adhesion properties. On the other hand, Zn – Sn-Cu3, Zn-Al15 – Sn-Cu3, Zn-Al15 – Sn-Zn30 and Al – Sn-Cu3 are the metallizations that exhibits better adhesion to the cell, and consequently, better mechanical properties. To improve the adhesion to the substrate, increasing the flow of the atomizing air will increase the viscous force and surface tension force.

3.2.5. Thermal conductivity

As aforementioned, to measure thermal conductivity, first it is necessary measure electrical conductivity. In Figure 3.23 is presented the evolution of the electrical conductivity with temperature for Sn-Zn30, Sn-Cu3, Zn, Zn-Al15, Zn ABM 225 μm and Zn ABM 800 μm .

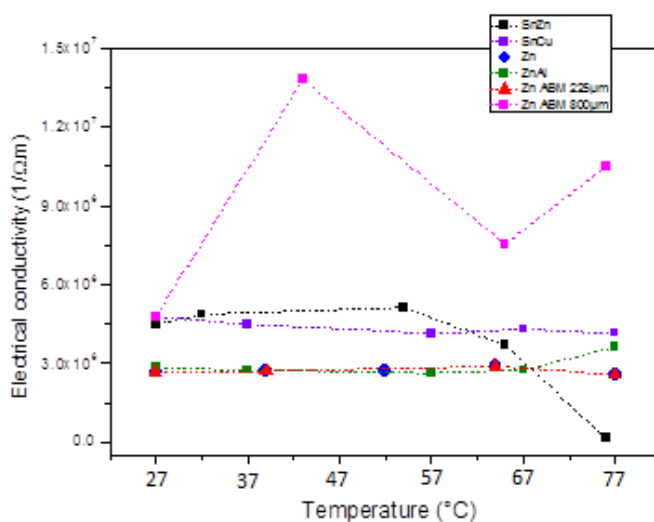


Figure 3.23 – Electrical conductivity evolution with temperature of Sn-Zn30, Sn-Cu3, Zn, Zn-Al15, Zn ABM 225 µm and Zn ABM 800 µm.

The electrical conductivity at 77 °C of Sn-Zn30, Sn-Cu3, Zn, Zn-Al15, Zn ABM 225 µm and Zn ABM 800 µm is presented in table 3.9.

Table 3.9 – Electrical conductivity results at 77 °C.

Sample	Electrical conductivity (1/Ω.m)
Sn-Zn30	1.90 × 10 ⁵
Sn-Cu3	4.16 × 10 ⁶
Zn	2.58 × 10 ⁶
Zn-Al15	3.62 × 10 ⁶
Zn ABM 225 µm	2.58 × 10 ⁶
Zn ABM 800 µm	1.05 × 10 ⁷

Sn-Zn30 is the sample that has the lowest value for electrical conductivity. On the other hand, Zn ABM 800 µm is the sample with the highest value of electrical conductivity, since it is the thickest. The Sn-Cu3, Zn, Zn-Al15 and Zn ABM 225 µm samples have approximately the same electrical conductivity value.

The thermal conductivity values at two temperatures for Sn-Zn30, Sn-Cu3, Zn, Zn-Al15, Zn ABM 225 µm and Zn ABM 800 µm are presented in Figure 3.24.

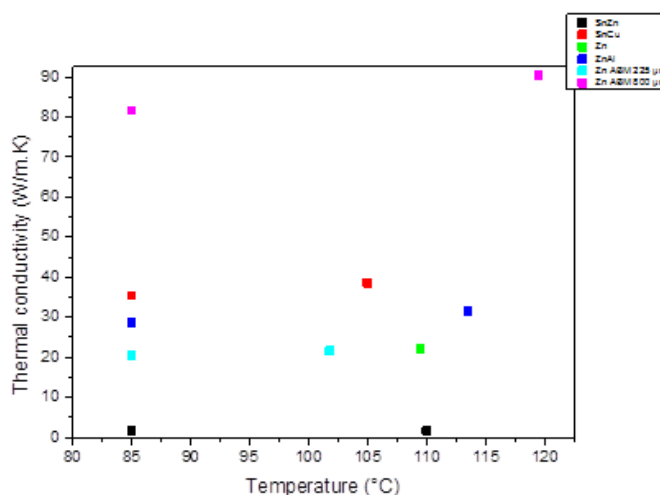


Figure 3.24 - Thermal conductivity at two different temperatures for Sn-Zn30, Sn-Cu3, Zn, Zn-Al15, Zn ABM 225 μm and Zn ABM 800.

In table 3.10 are presented the values for the two temperatures of thermal conductivity for Sn-Zn30, Sn-Cu3, Zn, Zn-Al15, Zn ABM 225 μm and Zn ABM 800.

Table 3.10 - Thermal conductivity values of Sn-Zn30, Sn-Cu3, Zn, Zn-Al15, Zn ABM 225 μm and Zn ABM 800.

	Temperature (°C)	k (W/m.K)	Temperature (°C)	k (W/m.K)
Sn-Zn30	85	1.62	110	1.69
Sn-Cu3	85	35.42	105	38.58
Zn	85	20.63	109.5	22.01
Zn-Al15	85	28.58	113.5	31.46
Zn ABM 225 μm	85	20.53	101.8	21.54
Zn ABM 800 μm	85	81.70	119.5	90.54

As expected, by increasing the temperature, the thermal conductivity increases. Sn-Zn30 is the sample with the lowest value of thermal conductivity, which means that is an appropriate material to use as thermal barrier coating. Zn, Zn ABM 225 μm and Zn-Al15 have similar values, and Sn-Cu3 has a higher value. This is probably due the good electrical conductivity of copper, which consequently, increases the thermal conductivity. Zn ABM 800 μm has the highest value, despite of its higher porosity.

CHAPTER 4 - Conclusions

4.1. Conclusions

Throughout this work, during the study of the film metallizations and metallizations used on top of the thin film capacitor cell, it was possible reach to some conclusions:

- In the electrochemical corrosion tests, there are some differences in the behavior of the film metallizations. F1 and F3, due to the presence of other elements in their composition, have lower corrosion potentials and thus lower corrosion resistance, however lower corrosion rate. On the other hand, F2 and F4 have higher corrosion resistance, but with higher corrosion rate.
- The difference between F5 and F6 film metallizations in the electrochemical corrosion tests does not explain the difference in the electrical behavior. Nevertheless, in the atomic force microscopy was found a significant difference in the average roughness value. F6 film metallization has higher average roughness value which leads to poor compaction at pressing stage, reducing the electrical contact between the films, and hence decreasing the electrical behavior.
- The in-flight particles of Sn-Cu₃, Sn-Zn₃₀, Zn, Al and Zn-Al₁₅ have different sizes (Zn and Al have the biggest particle sizes) and irregular shape with long and cylindrical particles. To avoid this and produce smaller particles with round and smooth surfaces it is necessary to increase the atomizing gas pressure.
- The porosity results showed that the Zn (electric arc) – Sn-Zn₃₀ sample has the higher porosity value due to the arc spray parameters are not optimized. Zn-Al₁₅ – Sn-Cu₃ is the sample with lower porosity level due probably to the smaller particles sizes of Zn-Al₁₅ and Sn-Cu₃. Comparing the zinc samples with different thicknesses produced by ABM machine, the sample with higher thickness (800 μm) has the higher porosity value due to higher amount of material deposited which increases the occurrence of defects. In the Zn-Al₁₅ – Sn-Cu₃ samples with different thicknesses, was found an optimum condition to process denser samples. The Zn-Al₁₅ (275 μm) – Sn-Cu₃ (325 μm) is the sample with lower porosity level, when compared with samples with higher and lower thicknesses.
- In terms of permeability, between Zn-Al₁₅, Zn, Sn-Zn₃₀ and Sn-Cu₃, the last two have the lowest permeability value, due to the smaller particles sizes. Smaller particles sizes, leads to denser coatings and thus, less permeable metallizations. In the samples produced by

ABM machine, as expected, the sample with lower thickness (225 μm) has the lower permeability value due to the less porosity level compared with the sample with 800 μm thickness. In the Zn-Al15 – Sn-Cu3 samples with different thicknesses, as the Zn-Al15 (275 μm) – Sn-Cu3 (325 μm) has the lowest porosity level, is the sample with the lowest permeability value.

- In the scratch test, the metallizations that revealed lower adhesion to the cell were Zn – Sn-Zn30 and Zn (electric arc) – Sn-Zn30. This means that Zn – Sn-Zn30 and Zn (electric arc) – Sn-Zn30 samples are those with worst mechanical adhesion properties. On the other hand, Zn – Sn-Cu3, Zn-Al15 – Sn-Cu3, Zn-Al15 – Sn-Zn30 and Al – Sn-Cu3 are the metallizations that exhibit better adhesion to the cell, and consequently, better mechanical properties. To improve the adhesion to the substrate, increasing the flow of the atomizing air will increase the viscous force and surface tension force, and thus the adhesion to the substrate.
- In thermal conductivity, increasing the temperature, the thermal conductivity increases. Zn ABM 800 μm has the highest value when was expected the contrary, which means that it is disadvantageous to use as thermal barrier coating. On the other hand, as Sn-Zn30 is the sample with lower value of thermal conductivity, is the sample more suitable to use as thermal barrier coating.

During this work, it was possible to conclude that the parameters of flame and arc spray are not optimized. With improved parameters it is possible to obtain smaller particles with round and smooth surfaces, which will produce denser metallizations with lower porosity level and hence, lower permeability. Nevertheless, the Zn-Al15 – Sn-Cu3 metallization is the better to protect the cell against humidity.

4.2. Future works

During this work, were studied the metallic materials that Vishay produces, and the results are satisfactory. However, as future works, probably would be of interest perform more characterization techniques in the metallizations such as:

- Micro hardness: to quantify the mechanical properties of the metallizations;
- Scanning electron microscopy (SEM): to observe with higher magnification the defects such as porosity or oxides.
- Energy dispersive X-ray Spectroscopy: to evaluate and quantify approximately the oxide content of the metallizations.

On the other hand, study more combination of metallizations processed by flame and arc spray and change the thickness of the layers, or even study the influence of only one layer may be of importance.

The major future work is probably improving the parameters of flame and arc spray and study the resulting metallizations. The parameters founded in literature are different than those used in Vishay, and, due to that, improving the parameters of flame and arc spray can be the solution to increase the tightness of the metallization and thus, increase the chances to the capacitor pass the biased 85°C/85% RH test.

REFERENCES

- [1] "Vishay - Company Info - About Vishay," 2012. [Online]. Available: <http://www.vishay.com/company/about/>. [Accessed: 14-Nov-2014].
- [2] M. Godec, D. Mandrino, and M. Gaberšček, "Investigation of performance degradation in metallized film capacitors," *Appl. Surf. Sci.*, vol. 273, pp. 465–471, May 2013.
- [3] V. Roederstein, "Film Capacitors," 2012 (products catalog).
- [4] R. M. Kerrigan and B. Kropiewnicki, "Film Capacitor Thermal Strategies Increase Power Density," Snow Hill, 2008.
- [5] J. Zhao and F. Liu, "Reliability assessment of the metallized film capacitors from degradation data," *Microelectron. Reliab.*, vol. 47, no. 2–3, pp. 434–436, Feb. 2007.
- [6] R. W. Kuehl, "Prediction and Acceleration Factors of Biased Humidity Testing of Thin Film Resistors," Heide, 2014.
- [7] C. Platt, *Encyclopedia of Electronic Components Volume 1*, First Edit. Sebastopol: O'Reilly Media, Inc., 2013.
- [8] KEMET, "Introduction to Capacitor Technologies," 2013 (local report).
- [9] F. Wang and Y. Wang, "Development and Utilization of Integral Thin Film Capacitors," *Procedia Environ. Sci.*, vol. 18, pp. 871–874, 2013.
- [10] E. J. Galvez, *Electronics with Discrete Components*, First Edit. USA: John Wiley & Sons, Inc., 2013.
- [11] W. J. Sarjeant, J. Zirnheld, and F. W. MacDougall, "Capacitors," *IEEE Trans. Plasma Sci.*, vol. 26, no. 5, pp. 1368–1392, 1998.
- [12] D. Stahler, "Types of Wound Film Capacitors," 2013 (local report).
- [13] M. Gebbia, "Introduction to film capacitors," 2015 (local report).
- [14] P. Viswanadham and P. Singh, *Failure Modes and Mechanisms in Electronic Packages*, First Edit. Boston, MA: Springer Science+Business Media Dordrecht, 1998.
- [15] V. Kumar, "Film Capacitors," Noida, 2010 (local report).
- [16] V. Intertechnology, *RFI suppression components*, First Edit. Vishay Intertechnology, Inc., 2002.

-
- [17] J. Smulko, K. Józwiak, M. Olesz, and L. Hasse, "Acoustic emission for detecting deterioration of capacitors under aging," *Microelectron. Reliab.*, vol. 51, no. 3, pp. 621–627, 2011.
- [18] G. Picci and M. Rabuffi, "Pulse handling capability of energy storage metallized film capacitors," *IEEE Trans. Plasma Sci.*, vol. 28, no. 5, pp. 1603–1606, 2000.
- [19] M. H. A. Malek, N. H. Saad, S. K. Abas, and N. M. Shah, "Thermal Arc Spray Overview," *IOP Conf. Ser. Mater. Sci. Eng.*, vol. 46, p. 012028, Jun. 2013.
- [20] V. Intertechnology, *Film capacitors - Vishay BCcomponents*, First Edit. Vishay Intertechnology, Inc., 2004.
- [21] P. Jain and E. J. Rymaszewski, *Thin-film capacitors for packaged electronics*. 2004.
- [22] M. A. Colwell, *Electronic components*. 1976.
- [23] B. S. Matisoff, *Handbook Of Elechronics Packaging Design and Engineering*. 1982.
- [24] D. Xin, L. Fuchang, L. Jin, and Zonggan Yao, "Influence factors for the self-healing of metallized polypropylene capacitors," *2000 Annu. Rep. Conf. Electr. Insul. Dielectr. Phenom.*, vol. 2, pp. 461–465, 2000.
- [25] A. C. Hall, J. F. Mccloskey, D. E. Beatty, H. A. P. li, L. H. Wyatt, and S. W. Othling, "Arc Spray Termination of Extended Foil Capacitors," Albuquerque and Livermore, 2012.
- [26] Z. Li, H. Li, F. Lin, Y. Chen, D. Liu, B. Wang, H. Li, and Q. Zhang, "Lifetime investigation and prediction of metallized polypropylene film capacitors," *Microelectron. Reliab.*, vol. 53, no. 12, pp. 1962–1967, Dec. 2013.
- [27] M. Rabuffi and G. Picci, "Status quo and future prospects for metallized polypropylene energy storage capacitors," *IEEE Trans. Plasma Sci.*, vol. 30, no. 5, pp. 1939–1942, Oct. 2002.
- [28] Metallization Ltd, "Introduction to Thermal Spray and Engineering Applications," 2013.
- [29] I. Gedzevicius and A. V. Valiulis, "Analysis of wire arc spraying process variables on coatings properties," *J. Mater. Process. Technol.*, vol. 175, no. 1–3, pp. 206–211, 2006.
- [30] J. R. Davis, *Handbook of thermal spray technology*, First Edit. USA: ASM International, 2004.
- [31] T. Lester and S. Milton, "Metallized coatings application," *Met. Finish.*, vol. 103, no. 7–8, pp. 35–38, 2005.

- [32] C. F. Yeung and D. Mei, "Investigation on the microstructure of spray coating," *J. Mater. Process. Technol.*, vol. 68, no. 3, pp. 275–278, Aug. 1997.
- [33] L. Pawlowski, *The Science and Engineering of Thermal Spray Coatings*. 2008.
- [34] "Thermal Spray Services | Thermal Spray | Hayden Corporation," 2015. [Online]. Available: http://www.haydencorp.com/content.php?p=flame_spray. [Accessed: 17-Jan-2015].
- [35] A. Arcondéguy, G. Gasgnier, G. Montavon, B. Pateyron, A. Denoirjean, A. Grimaud, and C. Huguet, "Effects of spraying parameters onto flame-sprayed glaze coating structures," *Surf. Coatings Technol.*, vol. 202, no. 18, pp. 4444–4448, 2008.
- [36] J. K. Chadwick, H. K. Wilson, and M. a. White, "An investigation of occupational metal exposure in thermal spraying processes," *Sci. Total Environ.*, vol. 199, no. 1–2, pp. 115–124, 1997.
- [37] N. Huonnic, M. Abdelghani, P. Mertiny, and A. McDonald, "Deposition and characterization of flame-sprayed aluminum on cured glass and basalt fiber-reinforced epoxy tubes," *Surf. Coatings Technol.*, vol. 205, no. 3, pp. 867–873, 2010.
- [38] M. P. Planche, H. L. Liao, and C. Coddet, "Relationships between in-flight particle characteristics and coating microstructure with a twin wire arc spray process and different working conditions," *Surf. Coatings Technol.*, vol. 182, no. 2–3, pp. 215–226, 2004.
- [39] Y. L. Zhu, H. L. Liao, C. Coddet, and B. S. Xu, "Characterization via image analysis of cross-over trajectories and inhomogeneity in twin wire arc spraying," *Surf. Coatings Technol.*, vol. 162, no. 2–3, pp. 301–308, 2003.
- [40] A. L. Johnston, A. C. Hall, and J. F. McCloskey, "Effect of Process Inputs on Coating Properties in the Twin-Wire Arc Zinc Process," *J. Therm. Spray Technol.*, vol. 22, no. 6, pp. 856–863, Jun. 2013.
- [41] "Thermal Spray Services | Thermal Spray | Hayden Corporation," 2015. [Online]. Available: http://www.haydencorp.com/content.php?p=arc_wire. [Accessed: 17-Jan-2015].
- [42] H. L. Liao, Y. L. Zhu, R. Bolot, C. Coddet, and S. N. Ma, "Size distribution of particles from individual wires and the effects of nozzle geometry in twin wire arc spraying," *Surf. Coatings Technol.*, vol. 200, no. 7, pp. 2123–2130, 2005.

- [43] R. Wang, D. Song, W. Liu, and X. He, "Effect of arc spraying power on the microstructure and mechanical properties of Zn-Al coating deposited onto carbon fiber reinforced epoxy composites," *Appl. Surf. Sci.*, vol. 257, no. 1, pp. 203–209, 2010.
- [44] T. Watanabe, X. Wang, E. Pfender, and J. Heberlein, "Correlations between electrode phenomena and coating properties in wire arc spraying," *Thin Solid Films*, vol. 316, no. 1–2, pp. 169–173, 1998.
- [45] H. C. Mi and D. Burger, "Accelerated lifetime-test for metallized film capacitors," Kaohsiung City, 2013.
- [46] D. Crowe and A. Feinberg, *Design for reliability*, First Edit. Boca Raton: CRC Press LLC, 2001.
- [47] C. W. Green, D. G. Clemons, W. R. Huber, and T. F. Mantz, "New Acceleration Factors for Temperature, Humidity, Bias Testing," *IEEE Trans. Electron Devices*, vol. 26, no. 1, pp. 56 – 71, 1979.
- [48] "1848 film capacitor." [Online]. Available: <http://www.vishay.com/images/product-images/pt-large/28164-pt-large.jpg>. [Accessed: 22-Jul-2015].
- [49] S. Santos, "Estágio," V. N. Famalicão, 2011.
- [50] G. Instruments, "Gamry Instruments Software Tutorials and Primers," 2005.
- [51] E. E. Stansbury and R. A. Buchanan, *Fundamentals of Electrochemical Corrosion*, First Edit. Ohio: ASM International, 2000.
- [52] P. L. Fauchais, J. V. R. Heberlein, and M. I. Boulos, *Thermal Spray Fundamentals - From powder to part*, First Edit. New York: Springer Science+Business Media, 2014.
- [53] P. L. Young, T. P. Brackbill, and S. G. Kandlikar, "Estimating Roughness Parameters Resulting From Various Machining Techniques for Fluid Flow Applications," *Proc. Fifth Int. Conf. Nanochannels, Microchannels Minichannels*, pp. 827–836, 2007.
- [54] "SEMAT." [Online]. Available: http://www.semat.lab.uminho.pt/Equipamento_1.htm. [Accessed: 22-Jul-2015].
- [55] "MatWeb: Zinc, Zn." [Online]. Available: <http://www.matweb.com/search/DataSheet.aspx?MatGUID=8909140a76074049809ad74d536ed606&ckck=1>. [Accessed: 21-Jul-2015].

- [56] “MatWeb: Aluminum, Al.” [Online]. Available: <http://www.matweb.com/search/DataSheet.aspx?MatGUID=0cd1edf33ac145ee93a0aa6fc666c0e0>. [Accessed: 21-Jul-2015].
- [57] “MatWeb: Tin, Sn.” [Online]. Available: <http://www.matweb.com/search/DataSheet.aspx?MatGUID=64d7cf04332e428dbca9f755f4624a6c>. [Accessed: 21-Jul-2015].
- [58] “MatWeb: Copper, Cu.” [Online]. Available: <http://www.matweb.com/search/DataSheet.aspx?MatGUID=ca486cc7cefa44d98ee67d2f5eb7d21f>. [Accessed: 21-Jul-2015].
- [59] ASTM, “Standard Test Methods for Water Vapor Transmission of Materials,” Philadelphia, 2002.
- [60] “SEMAT.” [Online]. Available: http://www.semat.lab.uminho.pt/Equipamento_5.htm. [Accessed: 21-Jul-2015].